Main Manuscript for

Characterization of *aliA* and *aliB* deletion mutants reveals a dominant role of AliA in *Haloferax volcanii* lipoprotein lipidation

Yirui Hong[1], Andy Garcia[2], Samuel Kopelev[3], Jacob A. Cote[1], Friedhelm Pfeiffer[4], Paula Welander[2], Stefan Schulze[3*], and Mechthild Pohlschroder[1*]

[1]Department of Biology, University of Pennsylvania, Philadelphia, Pennsylvania 19104, USA

[2]Department of Earth System Science, Stanford University, Stanford, California 94305, USA

[3]Thomas H. Gosnell School of Life Sciences, College of Science, Rochester Institute of Technology, Rochester, New York 14623, USA

[4]Computational Systems Biochemistry, Max Planck Institute of Biochemistry, 82152 Martinsried, Germany

Corresponding author: Mechthild Pohlschroder; Stefan Schulze

Email: pohlschr@sas.upenn.edu; stefan.schulze@rit.edu

ABSTRACT

Protein lipidation is a widespread strategy for anchoring proteins to cellular membranes across all domains of life, yet the mechanisms underlying this process in archaea remain poorly understood. Recently, the first archaeal enzymes involved in lipobox-containing protein (lipoprotein) biogenesis, AliA and AliB, were identified and characterized in the model archaeon *Haloferax volcanii*. Although these paralogs share significant sequence similarity, distinct deletion phenotypes suggest differences in their substrate specificity and function. Here, we employed large-scale Triton X-114 fractionation followed by quantitative proteomics and lipid-specific mass spectrometry to systematically analyze AliA- and AliB-dependent lipoprotein lipidation. Deletion of *aliA* affected substantially more lipoproteins in *Hfx. volcanii* than deletion of *aliB*, markedly diminishing their TX-114 enrichment—indicating reduced hydrophobicity—and abolishing thioether-linked archaeol modification. This establishes AliA as the primary enzyme responsible for archaeal lipoprotein lipidation. In contrast, deletion of *aliB* affected only a small subset of lipoproteins and did not significantly reduce thioether-linked archaeol levels. In addition to defining distinct and non-redundant roles for AliA and AliB, this study provides the first large-scale experimental validation of predicted archaeal lipoproteins and identifies candidate components of the archaeal lipoprotein biogenesis pathway, substantially advancing mechanistic understanding and enabling improved lipoprotein prediction in this previously underexplored field.

INTRODUCTION

Protein lipidation is a widely conserved phenomenon observed across all domains of life[1–4]. It significantly increases the hydrophobicity of proteins, thereby influencing their structures, stability, subcellular localization, enzymatic activities, and interactions with membranes and other proteins. Extensive studies in eukaryotes and bacteria have revealed a highly diverse landscape of lipidation types, each mediated by distinct enzymes and characterized by different conserved motifs, lipid anchors, biochemical properties, and biological functions[1–3,5]. In Archaea, a domain of life with important implications for eukaryogenesis[6–8], ecology[9,10], and biotechnology[11,12], protein lipidation exhibits distinct features compared to the other two domains. While two lipidation types commonly seen in eukaryotes and/or bacteria, GPI anchoring[13] and acylation[14–16], have also been reported in archaea, the predominant form of archaeal protein lipidation is

42 expected to be prenylation[17–24], the addition of isoprenoid-derived moieties to proteins. This preference is
43 likely attributed to the unique composition of archaeal membrane lipids, which are composed predominantly
44 of isoprenoid-based alkyl chains ether-linked to glycerol-1-phosphate backbones[25–27], in contrast to the fatty
45 acyl chains ester-linked to glycerol-3-phosphate backbones in eukaryotes and most bacteria[28–30].

46 Two major classes of prenylated proteins have been reported in archaea: the C-terminally lipidated ArtA
47 (archaeasortase A) substrates[20,21,23,24,31] and N-terminally lipidated proteins that contain a signature lipobox
48 motif ([L/V/I]$^{-3}$ [A/S/T/V/I]$^{-2}$ [G/A/S]$^{-1}$ [C]$^{+1}$)[4,32]. These lipobox-containing proteins are also widespread in
49 bacteria and are commonly referred to as bacterial lipoproteins in the literature[33,34]. In bacteria, lipoprotein
50 biogenesis begins with the transport of lipoprotein precursors to cell membranes either in an unfolded state
51 via the general secretory (Sec) pathway or in a folded state via the twin-arginine translocation (Tat)
52 pathway[35]. The maturation of bacterial lipoproteins is subsequently carried out through a highly conserved
53 three-step process. First, prolipoprotein diacylglyceryl transferase (Lgt) catalyzes the covalent attachment
54 of a membrane lipid moiety to the lipobox cysteine[36]. Next, the lipoprotein signal peptidase (Lsp) cleaves
55 the signal peptide N-terminal to the modified cysteine[37]. Finally, in some lipoproteins, the α-amino group of
56 the cysteine undergoes further lipidation by lipoprotein N-acyltransferase (Lnt)[38], lipoprotein *N*-acyl
57 transferase system A and B (LnsAB)[39], or lipoprotein intramolecular transacylase (Lit)[40]. A substantial
58 fraction of archaeal proteins contain a canonical lipobox motif with an essential cysteine and are therefore
59 considered to be archaeal lipoproteins[4,41]. However, despite this widespread genomic signature, only a
60 small number of predicted archaeal lipoproteins have been experimentally confirmed[4,42–44]. Moreover, no
61 homologs of the bacterial lipoprotein biosynthetic enzymes have been reported in archaea, consistent with
62 the substantial differences in membrane lipid composition between the two domains.

63 Recently, by combining bioinformatic analyses with biochemical characterization, we identified two
64 paralogous proteins, AliA and AliB, as the first known components of the archaeal lipoprotein biogenesis
65 pathway[43]. While AliB is restricted to Haloarchaea, AliA is widely conserved across archaeal species.
66 Deletion of *aliA* and/or *aliB* in the model archaeon *Haloferax volcanii* impaired lipoprotein biogenesis and
67 caused diverse physiological defects, including slower growth, decreased motility, and altered cell shape.
68 Deletion of both genes resulted in a complete loss of thioether-linked archaeol modification in lipoprotein

extracts, demonstrating AliA and/or AliB are essential for archaeal protein prenylation. Notably, Δ*aliA* showed more severe defects than Δ*aliB* in both lipoprotein biogenesis and cell physiology, and the defect of one could not be complemented by overexpressing the other, indicating different enzymatic activities of the two paralogs. One possible explanation is that AliA serves as the primary enzyme for forming the thioether-linked archaeol, similar to the case of model bacterium *Mycobacterium smegmatis*, where one Lgt homolog is substantially more active than the other[45,46]. This is further supported by the observation that two conserved arginine residues in AliA correlate with Lgt arginine residues known to be critical for binding to negatively charged membrane lipids[47,48], as revealed by visual structural comparison[43], whereas these positions are replaced by two histidines in AliB[43]. Alternatively, AliA may act on a broader set of substrates than AliB, even if both possess comparable catalytic activity.

Here, we aimed to uncover mechanisms underlying the phenotypic differences between Δ*aliA* and Δ*aliB*. Using large-scale Triton X-114 extraction and subsequent mass spectrometry (MS), we systematically assessed the lipidation status of predicted lipoproteins in wild-type and mutant *Hfx. volcanii* strains. This approach not only resolved the distinct substrate specificities of AliA and AliB, but also substantially expanded the catalog of archaeal proteins experimentally validated as lipoproteins. In parallel, lipid-specific mass spectrometry revealed a marked reduction in thioether-linked archaeol modifications in Δ*aliA*, but not in Δ*aliB*. Together, these findings establish AliA as the dominant contributor to lipoprotein lipidation in *Hfx. volcanii*.

RESULTS

Triton X-114 extraction enriched hydrophobic proteins in *Hfx. volcanii*

To determine substrate specificities of AliA and AliB in *Hfx. volcanii*, we set out to examine the lipidation status of lipobox-containing proteins (i.e. predicted lipoproteins, hereafter referred to as lipoproteins) and identify those with impaired lipidation in Δ*aliA*, Δ*aliB*, and Δ*aliA*/Δ*aliB*. Previously, we successfully used Triton X-114 (TX-114), a detergent widely used for extracting hydrophobic proteins in eukaryotes[49–51] and bacteria[52–54], to demonstrate lipidation of two archaeal lipoproteins[43]. TX-114 effectively separated the lipidated proteoforms in the detergent phase (TX phase) from their non-lipidated counterparts in the

aqueous phase (AQ phase). However, the efficiency of TX-114 for isolating archaeal lipoproteins in bulk has not been established so far. Therefore, we first performed TX-114 extraction in wild-type *Hfx. volcanii* (strain H53) and analyzed the proteome of the two phases via label-free, quantitative proteomics. About 64% of the 4222 predicted proteins encoded by *Hfx. volcanii* were quantified across the TX and AQ phases, a coverage in line with the most comprehensive single dataset in the Archaeal Proteome Project (ArcPP) (see Supplementary Fig.1 for a comparison of peptide and protein identifications)[55,56].

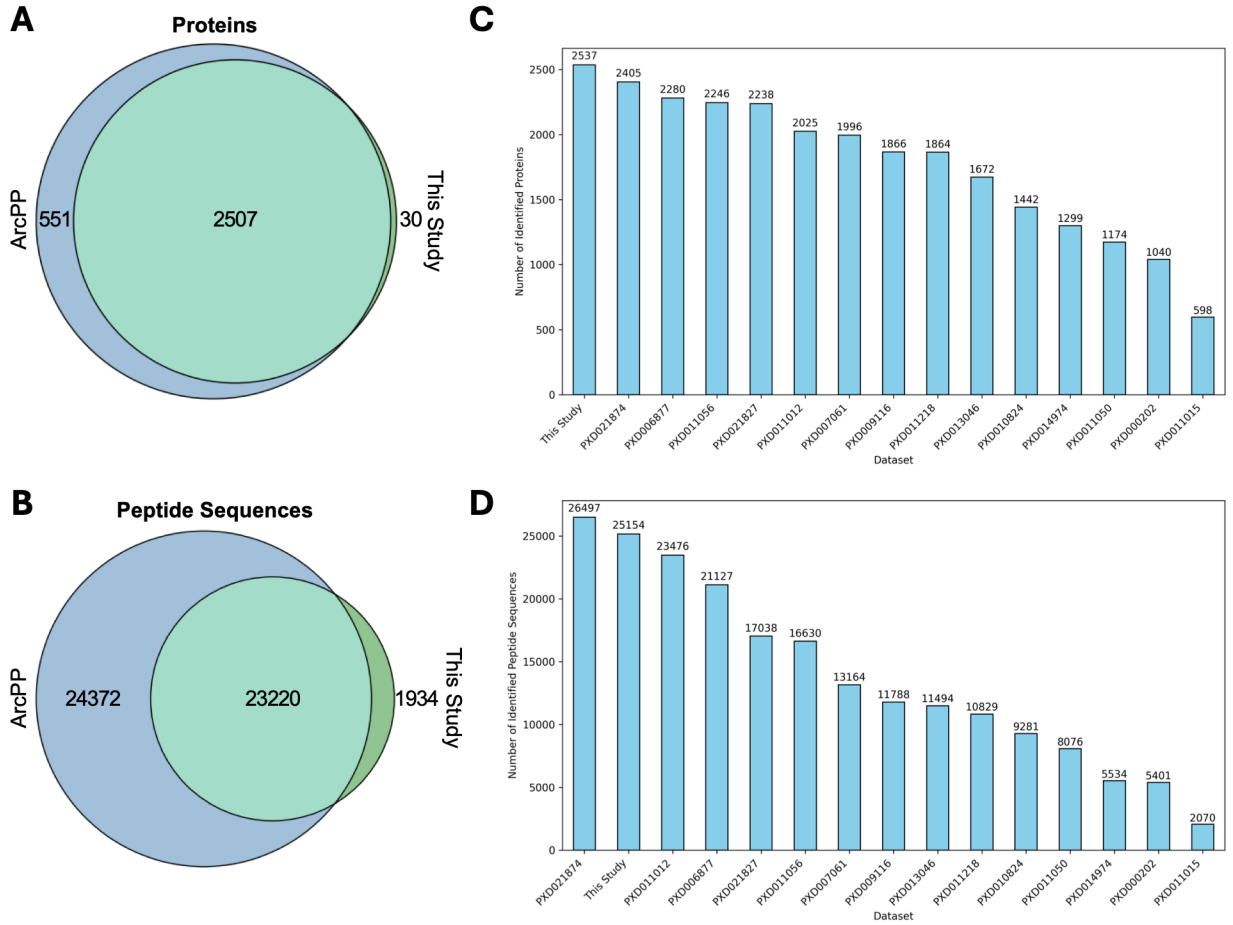

Supplementary Fig. 1. Proteome coverage comparison between this study and datasets within the Archaeal Proteome Project. Venn diagrams illustrating the overlap between **(a)** protein and **(b)** peptide identifications for this study and for the Archaeal Proteome Project (ArcPP, v. 1.4.0)[55]. Bar plots showing the number of identified **(c)** proteins and **(d)** peptides for this study and for each dataset in the ArcPP. The same filtering criteria were applied for all datasets (≤1% PEP on the peptide spectrum match level (PSM), ≤1% FDR on the peptide level, ≤0.5% FDR on the protein level, and at least 2 PSMs for each level). Notably,

108 out of the 30 proteins that were uniquely identified in this study, 18 are predicted to have ≥2 TM domains,
109 and 2 are predicted to be processed by a prepilin peptidase. These results indicate that fractionation with
110 Triton X-114 is beneficial for achieving high proteome coverage, including a high coverage of membrane
111 proteins. The dataset with the second-highest number of protein identifications and highest number of
112 peptide identifications (PXD021874), published later than the original ArcPP study, used subcellular
113 fractionation (cytosol, membrane, and culture supernatant) and two different enzymes for protein digestion
114 (trypsin and GluC)[56]. It should also be noted that an additional large-scale proteomics study[57] was published
115 while this manuscript was in preparation, achieving the highest protein and peptide coverage to date using
116 a different protein extraction and mass spectrometry workflow; the implementation of this recent dataset
117 into the ArcPP is pending.

118 We next examined the distribution of specific protein groups in the TX and AQ phases by comparing their
119 relative abundances. As a positive control, proteins with two or more predicted transmembrane domains
120 (hereafter referred to as ≥2 TM) were highly enriched in the TX phase (median $\log_2$FC of 3.71, Fig. 1a,b).
121 In contrast, the vast majority of predicted cytoplasmic proteins (hereafter referred to as Cyt, defined as
122 proteins lacking predicted transmembrane domains and secretion signals), as a negative control, were
123 more abundant in the AQ phase (median $\log_2$FC of -1.1, Fig. 1a,b). Consistent with the overall high
124 proteome coverage, 81% (87) of the 108 lipoproteins predicted by SignalP 6.0 with ≥90% confidence
125 (Supplementary Data 1) were quantified and were highly enriched in the TX phase, in line with the
126 anticipated behavior. Specifically, 72 (83%) of the 87 quantified lipoproteins were more abundant in the TX
127 phase (Fig. 1a), of which 13 were detected exclusively in the TX phase while 59 were strongly enriched
128 (Supplementary Table 1). Among lipoproteins showing significant abundance differences between the two
129 phases, the median $\log_2$FC was 4.93 (Fig. 1b), which was significantly higher (p-value < 10^{-10}) than that of
130 Cyt proteins ($\log_2$FC = - 1.10) and even slightly higher (p-value = 0.055) than that of ≥2 TM proteins ($\log_2$FC
131 = 3.71). Together, these results establish TX-114 extraction as an effective method to enrich hydrophobic
132 proteins, providing a foundation for its application in analyzing lipoproteins across strains.

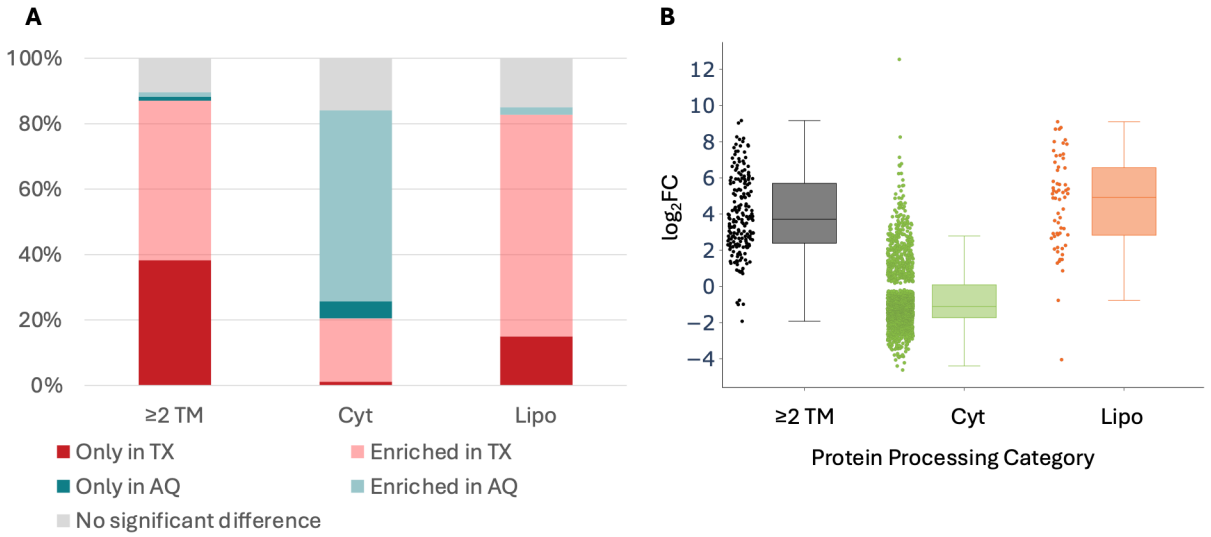

Fig. 1. TX-114 efficiently enriched hydrophobic proteins in wild-type *Hfx. volcanii* (strain H53). (a) The stacked bar graph indicates the percentage of proteins that were quantified only in the TX-114 (TX) or aqueous (AQ) phase, or enriched in either phase, or showing no significant difference between the phases. Percentages for each predicted protein group are normalized to the total number of quantified proteins within that group. ≥2 TM, proteins with at least two predicted transmembrane domains; Cyt, cytoplasmic proteins; Lipo, lipoproteins. **(b)** Log_2 fold-changes (FC) of protein abundance in TX versus AQ phase in wild-type *Hfx. volcanii* for different predicted protein groups are depicted as boxplots. Only proteins with significant abundance differences between the two phases are represented in the figure. Boxplots show the median (center line between boxes), interquartile range (boxes), as well as the range of data points within 1.5x of the interquartile range (whiskers).

Supplementary Table 1. Protein counts by predicted group and status in the mass spectrometry analysis of detergent (TX) and aqueous (AQ) phase in wild-type *Hfx. volcanii* (strain H53). The numbers of proteins that were quantified only in the TX or AQ phase, or enriched in either phase, or showing no significant difference between the phases are listed. “Total” corresponds to the numbers of proteins for each predicted group within the whole theoretical proteome. ≥2 TM, proteins with at least two predicted transmembrane domains; Cyt, cytoplasmic proteins; Lipo, lipoproteins.

Category	Total	Quantified	Only in TX	Enriched in TX	Only in AQ	Enriched in AQ	No significant difference
≥2 TM	784	384	147	187	5	5	40
Cyt	3112	2045	22	397	107	1190	326
Lipo	108	87	13	59	0	2	13

151 ***AliA* deletion significantly reduced overall lipoprotein hydrophobicity**

152 We next analyzed the protein profiles in the TX phase and AQ phase of Δ*aliA*, Δ*aliB*, and Δ*aliA*/Δ*aliB*.
153 Although the number of quantified lipoproteins was comparable across all strains (Fig. 2a, Supplementary
154 Table 2), the fraction of lipoproteins enriched or only quantified in the TX phase dropped from 82% (72 of
155 88) and 83% (73 of 88) in the wild type and Δ*aliB*, respectively, to 44% (39 of 88) and 42% (37 of 88) in
156 Δ*aliA*/Δ*aliB* and Δ*aliA*, respectively (Supplementary Table 2). Accordingly, lipoproteins in the *aliA* deletion
157 strains were increasingly enriched in the AQ phase or showed no significant difference between the two
158 phases (Fig. 2a, Supplementary Table 2). While around 40% of lipoproteins remained associated with the
159 TX phase in *aliA* deletion strains, this distribution does not necessarily indicate lipidation, as non-lipidated
160 lipoproteins may still associate with the TX phase via the hydrophobic domain (H-domain) of their uncleaved
161 signal peptides. Indeed, the median $\log_2$FC of lipoproteins showing significant abundance differences
162 between the two phases decreased from 4.93 in the wild type to 1.02 in Δ*aliA*/Δ*aliB* and 1.10 in Δ*aliA*,
163 reflecting an approximately 16-fold reduction in TX phase enrichment relative to the AQ phase, and thus a
164 significant decrease in lipoprotein hydrophobicity (Fig. 2b, p-values $< 10^{-10}$ for both strains compared to the
165 wild type). In contrast, Δ*aliB* showed no significant change in $\log_2$FC (5.34 versus 4.93 in wild type, p-value
166 = 0.84, Fig. 2b), suggesting that AliB has a much narrower substrate range than AliA or may function in
167 processes other than lipidation. It should also be noted that no significant change in the TX/AQ distribution

168 was observed for proteins with ≥2 TM domains in any of the mutant strains, indicating that the reduced
169 protein hydrophobicity in Δ*aliA* and Δ*aliA*/Δ*aliB* is specific to lipoproteins (Fig. 2b).

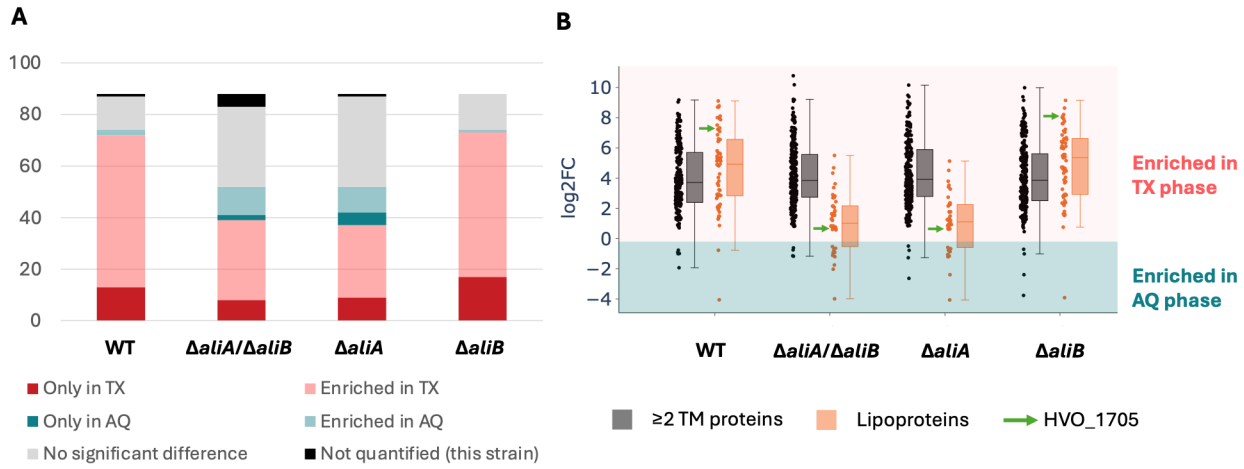

170

171 **Fig. 2. Deletion of *aliA*, but not *aliB*, significantly reduced the number of TX-enriched lipoproteins.**
172 **(a)** Number of lipoproteins quantified only in the TX-114 (TX) or aqueous (AQ) phase, or enriched in either
173 phase, or showing no significant difference between the phases, across different strains. "Not quantified
174 (this strain)" corresponds to the number of lipoproteins that have been quantified in other strains but not in
175 the respective strain. **(b)** Log_2 fold-changes (FC) of protein abundance in TX versus AQ phase in the
176 analyzed strains for lipoproteins and ≥2 TM proteins (having at least two predicted transmembrane
177 domains). Only proteins with significant abundance differences are represented in the figure. HVO_1705 is
178 a verified Tat-transported lipoprotein[43]. Boxplots show the median (center line between boxes), interquartile
179 range (boxes), as well as the range of data points within 1.5x of the interquartile range (whiskers).

180 **Supplementary Table 2. Counts of *Hfx. volcanii* lipoproteins by enrichment status across strains.**
181 The numbers of proteins that were quantified only in the TX or AQ phase, or enriched in either phase, or
182 showing no significant difference between the phases, or not quantified in the respective strain, are listed.
183 "Total" refers to the number of lipoproteins quantified across all strains. "Not quantified (this strain)" refers
184 to numbers of proteins that were detected in the whole MS dataset included in this study but were not
185 quantified in the specific strain shown.

Strains	Total	Quantified	Only in TX	Enriched in TX	Only in AQ	Enriched in AQ	No significant difference	Not quantified (this strain)

WT	88	87	13	59	0	2	13	1
Δ*aliA*/Δ*aliB*	88	83	8	31	2	11	31	5
Δ*aliA*	88	87	9	28	5	10	35	1
Δ*aliB*	88	88	17	56	0	1	14	0

186

187 **Large-scale proteomic validation of the predicted *Hfx. volcanii* lipoproteome**

188 While several studies have predicted the prevalence and abundance of lipoproteins in archaea[4,41,43], only
189 a limited number of predicted lipoproteins have been experimentally validated[4,42–44]. To confirm additional
190 lipoproteins, we applied a three-step validation strategy. First, we selected predicted lipoproteins that, in
191 the wild-type sample, were significantly enriched in the TX phase compared to the AQ phase. From this
192 subset, we identified proteins showing a significant reduction (at least 1.5-fold) of TX phase abundance in
193 any of the three *ali* mutants compared to the wild type (defined as log2FC of TX_{mut}:TX_{WT} < -0.58). Third, we
194 excluded proteins that also exhibited reduced abundance in mutant AQ phase, thereby removing those
195 non-lipoproteins with globally decreased expression in *ali* mutants and minimizing false positives. Together,
196 this pattern was interpreted as indicative of reduced protein hydrophobicity in *ali* mutants and as supporting
197 evidence for lipoprotein identity.

198 To validate this approach, we first assessed how previously verified lipoproteins performed in this analytical
199 workflow. Four previously confirmed *Hfx. volcanii* lipoproteins met these criteria (Supplementary Data 2),
200 supporting the robustness of the method. This included HVO_1245, which is predicted as cytoplasmic by
201 SignalP 6.0 and would have been excluded based solely on prediction; however, our MS data supports its
202 lipoprotein identity, highlighting the potential of this method for improving prediction tools. In line with the
203 reliability of our approach, HVO_1808, a predicted Sec lipoprotein previously shown to be processed even
204 when its lipobox cysteine was mutated[4], did not pass the filter and displayed similar TX phase enrichment
205 across all strains, suggesting its SignalP 6.0 lipoprotein prediction is likely a false positive (Supplementary
206 Data 2).

207 Having validated the workflow, we applied it to all 88 predicted lipoproteins quantified across the dataset.
208 After applying the three selection criteria, 51 proteins remained, supporting their predictions as lipoproteins

209 (Fig. 3a). Most (40 out of 51) showed reduced hydrophobicity in strains lacking *aliA* (Δ*aliA* and Δ*aliA*/Δ*aliB*),
210 but not in Δ*aliB* (Fig. 3a, Supplementary Table 3), indicating that AliB is involved in the lipidation of
211 substantially fewer *Hfx. volcanii* lipoproteins than AliA. This group includes HVO_1705, a previously
212 characterized lipoprotein that showed impaired lipidation in Δ*aliA* and Δ*aliA*/Δ*aliB* but remained largely
213 unaffected in Δ*aliB*[43] (Fig. 2B). In addition, five lipoproteins were uniquely affected in Δ*aliA* and three in
214 Δ*aliA*/Δ*aliB* (Fig. 3a, Supplementary Table 3), suggesting minor differences between the two mutants. Of
215 the three AliB substrates identified, one was affected only in Δ*aliB* (Fig. 3a, Supplementary Table 3).

216 Because the three-step workflow required statistical comparisons between TX and AQ phases in the wild
217 type and between TX phases of wild type and mutant strains, proteins had to be quantified in all relevant
218 fractions to meet the significance criteria. Consequently, proteins with missing values in either the AQ phase
219 of the wild type or the TX phase of the mutant could not be evaluated in the initial analysis. However, such
220 missing values are themselves consistent with strong phase enrichment and therefore consistent with
221 lipoprotein behavior. We therefore applied extended criteria to capture these cases, resulting in the
222 identification of seven additional validated lipoproteins (Fig. 3b, Supplementary Table 3). In addition, one
223 protein included in Fig. 3b had already been identified in Fig. 3a, as it was detected in Δ*aliA*/Δ*aliB* in the
224 first analysis but met the extended detection criteria only for Δ*aliA* in this subset (Supplementary Table 3).
225 Among the eight proteins, six exhibited reduced hydrophobicity in both Δ*aliA* and Δ*aliA*/Δ*aliB*, while two
226 were affected only in Δ*aliA* (Fig. 3b, Supplementary Table 3). Together, these results significantly expand
227 the set of validated *Hfx. volcanii* lipoproteins from fewer than ten to over fifty and further underscore the
228 marked difference in lipidation capacity between AliA and AliB.

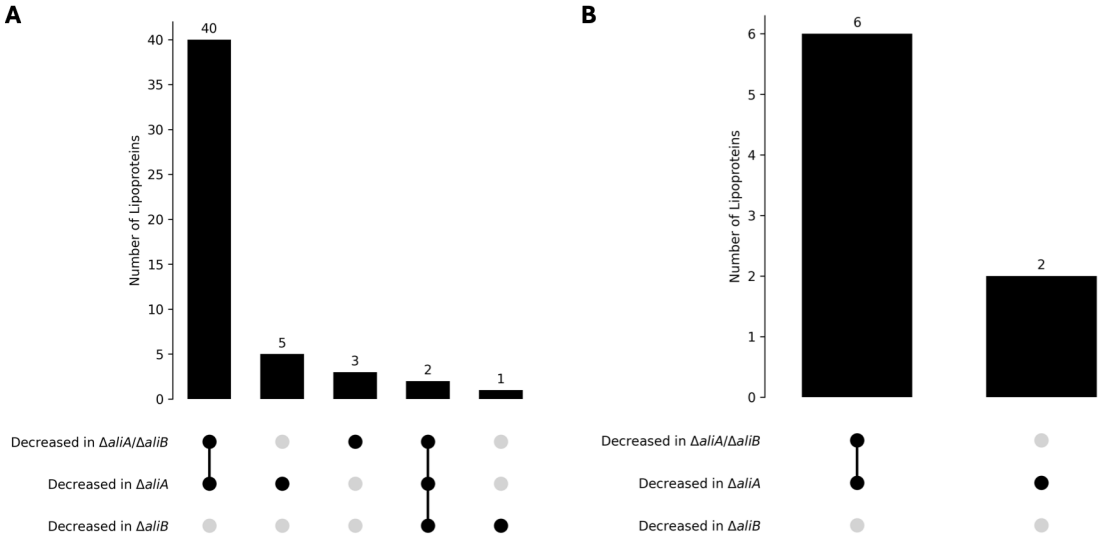

Fig. 3. Large-scale identification of lipoproteins through their reduced TX-phase abundance in *ali* deletion strains. (a) Numbers of lipoproteins that were enriched in wild-type TX phase and exhibited at least a 1.5-fold reduction in TX phase abundance in Δ*aliA*/Δ*aliB*, Δ*aliA*, or Δ*aliB* compared to the wild type, but were not significantly decreased in the corresponding AQ phase. These proteins are considered validated lipoproteins. **(b)** Numbers of lipoproteins identified using the extended criteria, including those not quantified in the wild-type AQ phase or the mutant TX phase.

Supplementary Table 3. Lipoproteins validated through their reduced TX-phase abundance in *ali* deletion strains. Predicted lipoproteins were considered validated if they were enriched in the TX phase of wild type and showed at least a 1.5-fold reduction in TX phase abundance in Δ*aliA*/Δ*aliB*, Δ*aliA*, or Δ*aliB* compared to the wild type, but were not significantly decreased in the corresponding AQ phase. Proteins are grouped based on whether they were quantified in all relevant conditions for comparison (Fig. 3a) or showed missing values in either the wild-type AQ phase or the mutant TX phase (Fig. 3b). *HVO_B0034 was identified in both analyses but met the detection criteria only for Δ*aliA*/Δ*aliB* in the Fig. 3a analysis and only for Δ*aliA* in the Fig. 3b analysis.

Proteins quantified in all relevant conditions (Fig. 3a)		
Category	**Count**	**Proteins**
Decreased in Δ*aliA* and Δ*aliA*/Δ*aliB*	40	HVO_0062, HVO_0447, HVO_0530, HVO_0628, HVO_1007, HVO_1240, HVO_1241, HVO_1242, HVO_1244, HVO_1401, HVO_1477, HVO_1603, HVO_1705, HVO_1888, HVO_2094, HVO_2153, HVO_2316, HVO_2375, HVO_2432, HVO_2607, HVO_2695, HVO_2798, HVO_A0181, HVO_A0283, HVO_A0324, HVO_A0362, HVO_A0428, HVO_A0611, HVO_A0619, HVO_A0620, HVO_A0623, HVO_A0627, HVO_B0021, HVO_B0047, HVO_B0082, HVO_B0093, HVO_B0138, HVO_B0292, HVO_B0328, HVO_C0075
Decreased in Δ*aliA* only	5	HVO_1673, HVO_1806, HVO_2651, HVO_B0106, HVO_B0198
Decreased in Δ*aliA*/Δ*aliB* only	3	HVO_B0034, HVO_B0139, HVO_B0318
Decreased in Δ*aliA*/Δ*aliB*, Δ*aliA*, and Δ*aliB*	2	HVO_0807, HVO_A0380
Decreased in Δ*aliB* only	1	HVO_B0184
Proteins missing in either WT AQ phase or the mutant TX phase (Fig. 3b)		
Category	**Count**	**Proteins**

Decreased in Δ*aliA* and Δ*aliA*/Δ*aliB*	6	HVO_1119, HVO_1144, HVO_2286, HVO_A0549, HVO_B0144, HVO_B0228
Decreased in Δ*aliA* only	2	HVO_A0557, HVO_B0034*

245 **Localization and abundance of the Tat lipoprotein HVO_1705 differ between Δ*aliA* and Δ*aliB***

246 Building on the global differences observed across the lipoproteome, we next focused on an individual
247 lipoprotein to further explore the distinct roles of AliA and AliB. Current proteomic data indicate that deletion
248 of *aliA*, but not *aliB*, significantly affects the lipidation of the lipoprotein HVO_1705 (Fig. 2B, Supplementary
249 Table 3). This is consistent with previous Western blot analyses, which suggest that deletion of *aliB* has
250 only a minor effect on HVO_1705 lipidation but a more pronounced effect on its signal peptide cleavage[43].
251 Together, these observations highlight HVO_1705 as a suitable model for dissecting AliA- and AliB-
252 dependent steps in lipoprotein biogenesis. We therefore attempted to purify HVO_1705 for direct MS
253 analysis of both peptides and lipid modifications. Although purification was limited by low protein abundance
254 and purity, during the process, we observed pronounced differences in its cellular localization among strains.
255 Cell fractionation of strains overexpressing HVO_1705 showed that the protein was predominantly
256 membrane-associated in the wild type (Fig. 4a). In contrast, in both Δ*aliA*/Δ*aliB* and Δ*aliA* strains,
257 HVO_1705 was primarily detected in the cytoplasmic fraction and exhibited reduced overall abundance
258 (Fig. 4a,b). These observations suggest that *aliA* deletion either impairs membrane targeting of
259 overexpressed HVO_1705 or triggers the clearance of non-lipidated HVO_1705 from both the membrane
260 and cytoplasm via an unidentified quality-control mechanism. Conversely, in the Δ*aliB* strain, the majority
261 of HVO_1705 remained membrane-associated, including both the mature form and the presumed lipidated
262 but non-cleaved intermediate form previously reported[43]. This pattern further confirmed that AliB contributes
263 more prominently to signal peptide cleavage than to lipidation of HVO_1705. As a control, we examined
264 the Tat-translocated non-lipoprotein HVO_0844, which is membrane-anchored by a C-terminal
265 transmembrane segment rather than covalent lipid modification. Its membrane localization was unaffected
266 by deletion of *aliA* or *aliB* (Fig. 4c,d), confirming that the localization effect observed in the mutants is

267 specific to lipoproteins. Collectively, these results further highlight the distinct roles of AliA and AliB and
268 suggest that *aliA* deletion may additionally reduce lipoprotein abundance through a mechanism that
269 remains to be elucidated.

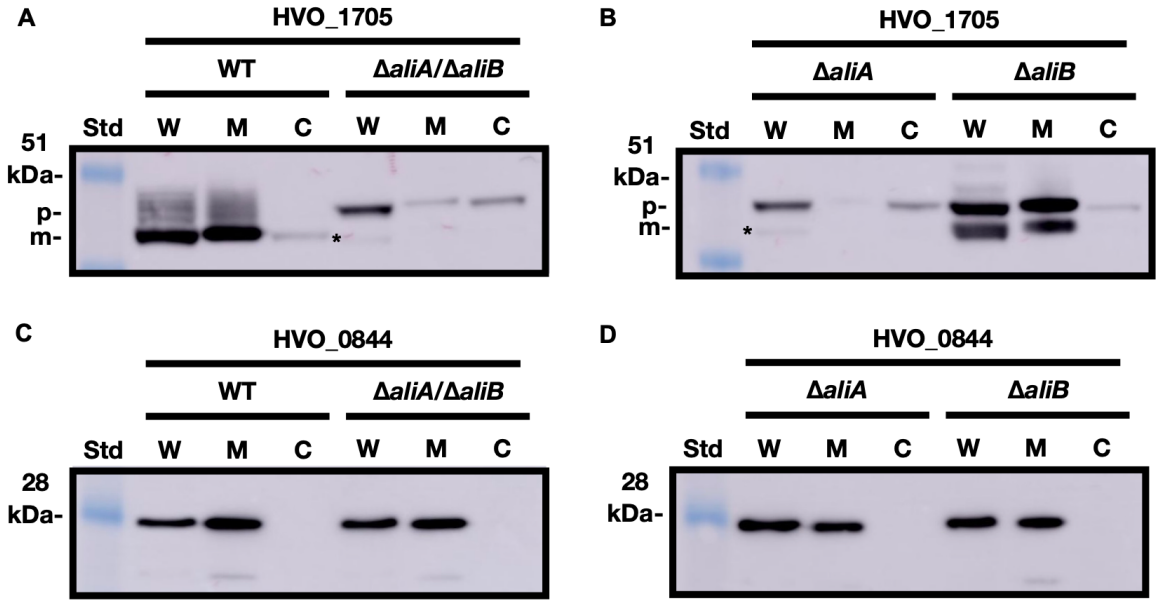

270

271 **Fig. 4. Deletion of *aliA*, but not *aliB*, led to a significantly reduced amount of membrane-associated**
272 **HVO_1705, while the Tat-transported transmembrane protein HVO_0844 was unaffected by either**
273 **deletion.** Western blot of overexpressed myc-tagged HVO_1705 in **(a)** wild type, Δ*aliA*/Δ*aliB*, **(b)** Δ*aliA*, and
274 Δ*aliB* in different cell fractions across strains. Western blot of overexpressed myc-tagged HVO_0844 in **(c)**
275 wild type, Δ*aliA*/Δ*aliB*, (**d)** Δ*aliA*, and Δ*aliB* in different cell fractions across strains. Std, SeeBlue Plus2 pre-
276 stained protein standard. W, whole cell lysates. M, membrane fraction. C, cytoplasmic fraction. Precursors
277 (p) and mature proteins (m) are labeled accordingly. The asterisk indicates a likely degradation product of
278 HVO_1705, as previously reported by Giménez et al[42]. The results are representative of two independent
279 experiments. The original blots for panels a-d are included in the Source Data file.

280 **AliA is the main enzyme for thioether-linked archaeol modification of *Hfx. volcanii* lipoproteins**

281 The results presented above focused on dissecting the differences between AliA and AliB using protein-
282 based readouts. To complement these findings, we next examined their roles by directly analyzing lipid

283 modifications across different strains. Previously, we showed that the TX-114 extract from the wild type
284 contained methylthio-archaeol, the cleavage product of thioether-linked archaeol following methyl iodide
285 treatment, whereas this modification was absent in Δ*aliA*/Δ*aliB*[43]. To determine which enzyme was
286 responsible for this phenotype, we performed liquid chromatography-mass spectrometry (LC-MS) analysis
287 of lipids isolated from TX-114 extracts of Δ*aliA* and Δ*aliB* strains. Deletion of *aliA* alone resulted in the
288 complete absence of methylthio-archaeol, while deletion of *aliB* did not reduce the level of thioether-linked
289 archaeol modification. This result correlates well with our observation that deletion of *aliA* reduced the
290 hydrophobicity of substantially more *Hfx. volcanii* lipoproteins than deletion of *aliB* (Fig. 3). Thus, the loss
291 of this lipid modification in the Δ*aliA*/Δ*aliB* strain[43] is primarily attributable to *aliA* deletion, underscoring the
292 essential role of AliA in mediating this lipid modification (Fig. 5a). Importantly, the absence of thioether-
293 linked archaeol modification in Δ*aliA* was not due to impaired archaeol synthesis, as total lipid profiles were
294 comparable across all strains, including the wild type (Fig. 5b).

295 Unexpectedly, while deletion of *aliB* did not reduce the level of thioether-linked archaeol modification, it
296 resulted in a slight increase in methylthio-archaeol levels compared to the wild type (p-value = 0.077, Fig.
297 5a). To resolve this, we quantified the AliA abundance in the analyzed strains and detected an increased
298 AliA abundance in the absence of AliB. Quantitative PCR (Supplementary Fig. 2, p-value = 0.174) and
299 proteomics data both indicated increased AliA levels in Δ*aliB*. Specifically, the $\log_2$FC of Δ*aliB* TX phase
300 versus wild-type TX phase was 1.11 (adjusted p-value = 0.07) and 1.60 in the AQ phase (adjusted p-value
301 = 0.04; see Data Availability for more raw data), pointing to potential functional crosstalk between AliA and
302 AliB.

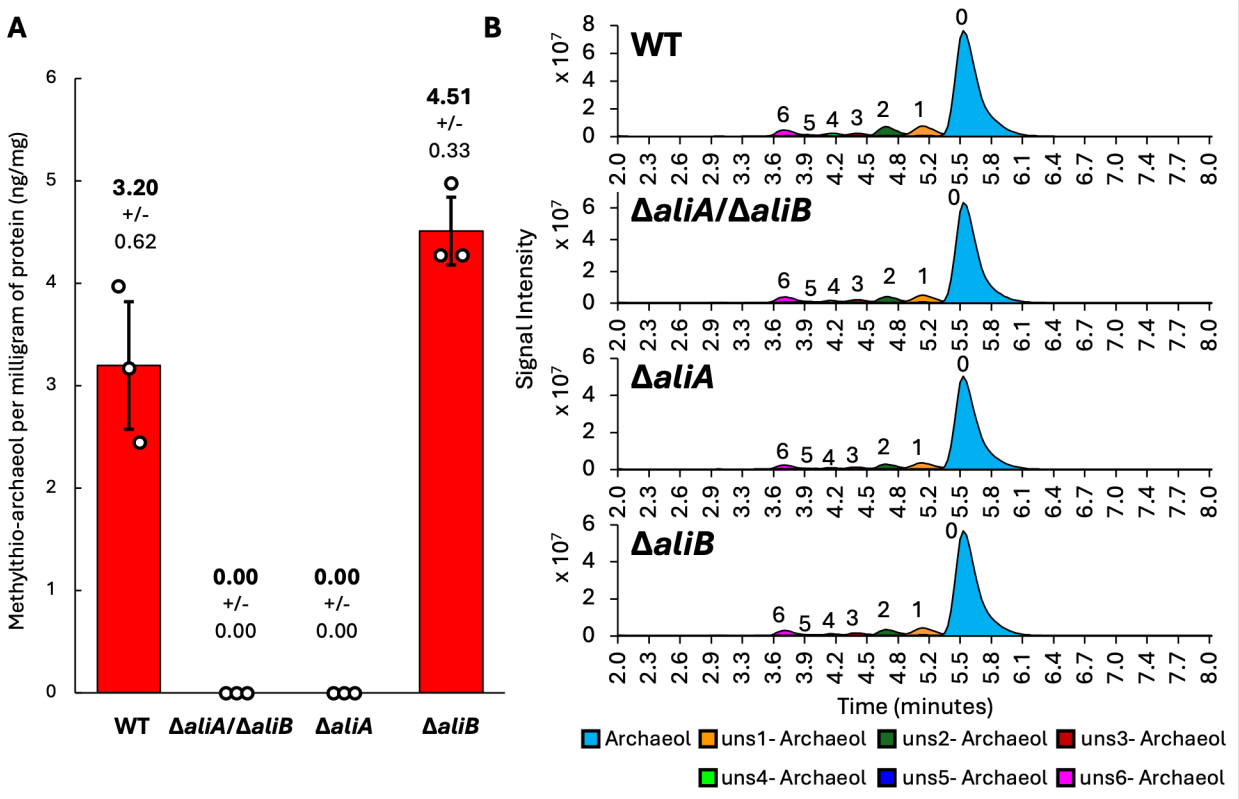

Fig. 5. Deletion of *aliA*, rather than *aliB*, led to the complete absence of thioether-linked archaeol in lipoprotein extracts. (a) Bar chart showing the average mass of methylthio-archaeol recovered from methyl iodide treated lipoproteins per milligram of starting protein, based on three biological replicates. Error bars represent standard deviations. Statistical significance was assessed using a two-tailed unpaired t-test assuming unequal variances (Welch's t-test) for comparison between the wild type and Δ*aliB* ($p = 0.077$). **(b)** As a control, the total lipids of each strain were analyzed. Representative merged extracted ion chromatograms (EICs, m/z values listed in Methods) show comparable relative abundances of saturated and unsaturated diether core lipids (archaeols) in base hydrolyzed biomass from the wild type, Δ*aliA*, Δ*aliB*, and Δ*aliA*/Δ*aliB*.

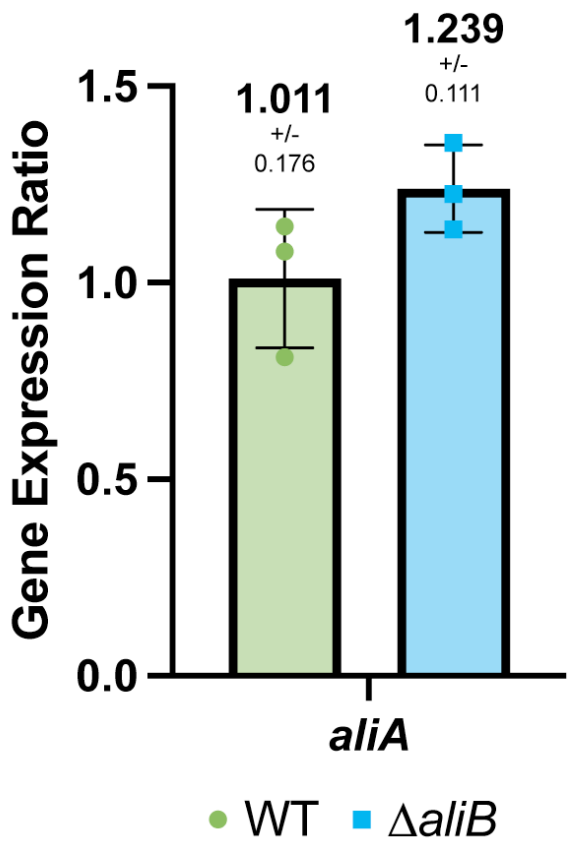

313

314 **Supplementary Fig. 2. Quantitative PCR showed a slight but non-significant increase in *aliA***
315 **expression in Δ*aliB* compared to the wild type (WT) (p-value = 0.174),** Bar height represents the mean
316 gene expression ratio normalized to an internal control gene. Error bars indicate standard deviation from
317 three biological replicates. Statistical significance was assessed using a two-tailed unpaired t-test assuming
318 unequal variances (Welch's t-test) for comparison between the log-transformed gene expression ratios of
319 wild type and Δ*aliB*.

320 **Downstream effects of *aliA* and *aliB* deletion beyond lipoproteins**

321 Given that lipoproteins participate in diverse cellular processes (Supplementary Data 1), disruption of
322 lipoprotein biogenesis is expected to exert pleiotropic effects extending beyond lipoproteins themselves.
323 Identifying non-lipoproteins whose abundance changes upon *aliA* or *aliB* deletion may therefore provide
324 insight into the molecular basis of the phenotypes observed in Δ*ali* mutants. Moreover, such proteins may
325 represent previously unrecognized components of the archaeal lipoprotein biogenesis pathway. We
326 therefore examined the impact of *aliA* and *aliB* deletion on non-lipoproteins associated with either the TX

327 phase or the AQ phase. TX-associated proteins were defined based on TX vs AQ comparisons within each
328 strain. Proteins exhibiting significant finite $\log_2$ fold enrichment in TX relative to AQ (i.e., detected in both
329 phases but enriched in TX) are shown in Fig. 6a–c (Supplementary Data 3-5). In contrast, proteins detected
330 exclusively in the TX phase—resulting in infinite $\log_2$ fold changes due to missing data in the AQ phase—
331 are shown in Fig. 6d–f (Supplementary Data 6-8). Because these latter comparisons rely on
332 presence/absence behavior and missing values, they are less quantitatively robust than finite enrichment
333 ratios, but they nevertheless highlight strongly phase-specific proteins.

334 Across all comparisons, a substantial set of non-lipoproteins exhibited significant abundance differences
335 between wild-type and mutant *Hfx. volcanii* strains (Fig. 6, Supplementary Fig. 3, Supplementary Data 3-
336 9). The most pronounced differences were observed in the TX phase (Fig. 6, Supplementary Data 3-8),
337 whereas the AQ phase displayed comparatively fewer and generally more moderate changes
338 (Supplementary Fig. 3, Supplementary Data 9). This pattern indicates that disruption of Ali-dependent
339 lipidation primarily perturbs the membrane-associated proteome rather than the soluble protein pool.
340 Among the TX-associated proteins, the archaellin subunit protein ArlA1 (HVO_1210) was enriched in the
341 detergent phase of all strains but showed reduced abundance in the TX phase of the mutants compared to
342 the wild type (Fig. 6a-c), providing a molecular explanation for their motility defects previously reported[43].
343 In addition, a large number of transport proteins were more abundant in the TX phase of the mutant strains
344 than in the wild type (Fig. 6), likely reflecting a downstream response to impaired lipidation of ABC substrate-
345 binding proteins, many of which are predicted to be lipoproteins (Supplementary Data 1).

346 Previously, we identified a comprehensive set of arCOGs (Archaeal Clusters of Orthologous Genes)[58,59]
347 that most frequently co-occur with lipoproteins as promising candidates for archaeal lipoprotein biogenesis
348 components, including arCOG02177 (*aliA*)[43]. We therefore assessed whether the top 25 arCOGs from the
349 list were differentially represented between mutant and wild-type strains. Among these, HVO_A0045
350 (arCOG01331), encoding an HtpX-like protease, showed reduced abundance in Δ*aliA* when taking only
351 finite $\log_2$ fold changes into account (Fig. 6b). When proteins that were only detected in the TX phase were
352 also considered, decreased abundance of HVO_A0045 was additionally observed in Δ*aliA*/Δ*aliB* and Δ*aliB*
353 strains (Fig. 6d,f). Bacterial HtpX homologs are implicated in the degradation of misfolded envelope proteins

354 and undergo self-cleavage upon membrane perturbation, suggesting that altered abundance of this
355 protease may reflect changes in envelope protein homeostasis following disruption of Ali-dependent
356 lipidation. Furthermore, when proteins only detected in the TX phase were included in the analysis,
357 HVO_2870 (arCOG02642), a predicted autoinducer-2 exporter (AI-2E) family protein, exhibited increased
358 abundance specifically in the Δ*aliA*/Δ*aliB* strain. Members of the AI-2E protein family have been reported
359 to function either in exporting the quorum sensing molecule autoinducer-2[60] or as Na^+ (Li^+)/H^+ antiporter[61].
360 Whether the altered abundance of these proteins reflects direct consequences of Ali pathway disruption,
361 indirect effects stemming from impaired lipoprotein maturation and associated cellular stress, or loss of
362 function of individual lipoproteins remains to be resolved. Finally, we analyzed the abundance of ArtA
363 substrates and ArtA itself in the mutants. No significant differences were detected for either, suggesting
364 that the ArtA-dependent prenylation pathway operates largely independent of the AliA/AliB-dependent
365 lipoprotein lipidation pathway in *Hfx. volcanii*.

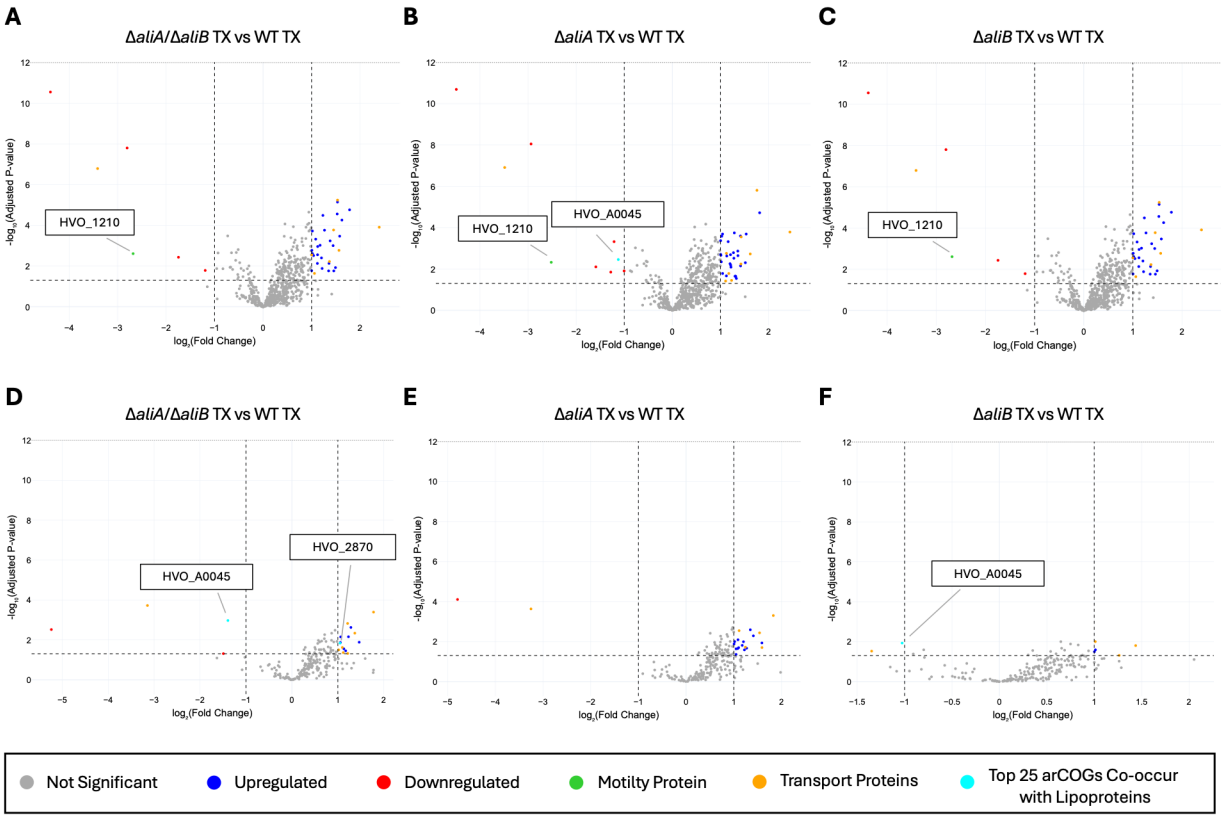

366

367 **Fig. 6. Deletion of *aliA* and *aliB* predominantly perturbs TX-associated non-lipoproteins.** Volcano
368 plots show proteins in the TX phase of (a,d) Δ*aliA*/Δ*aliB*, (b,e) Δ*aliA*, and (c,f) Δ*aliB* compared to wild-type
369 *Hfx. volcanii*. Panels a–c display proteins exhibiting significant finite $\log_2$ fold enrichment in TX relative to
370 AQ within each strain (i.e., detected in both fractions but enriched in TX). Panels d–f display proteins
371 detected exclusively in the TX phase of at least one strain, resulting in infinite $\log_2$ fold changes due to
372 absence from the AQ phase. Proteins with $|\log_2 FC| > 1$ and adjusted p-value < 0.05 are considered
373 significantly differentially abundant. Selected groups of differentially abundant proteins are highlighted in
374 distinct colors as indicated.

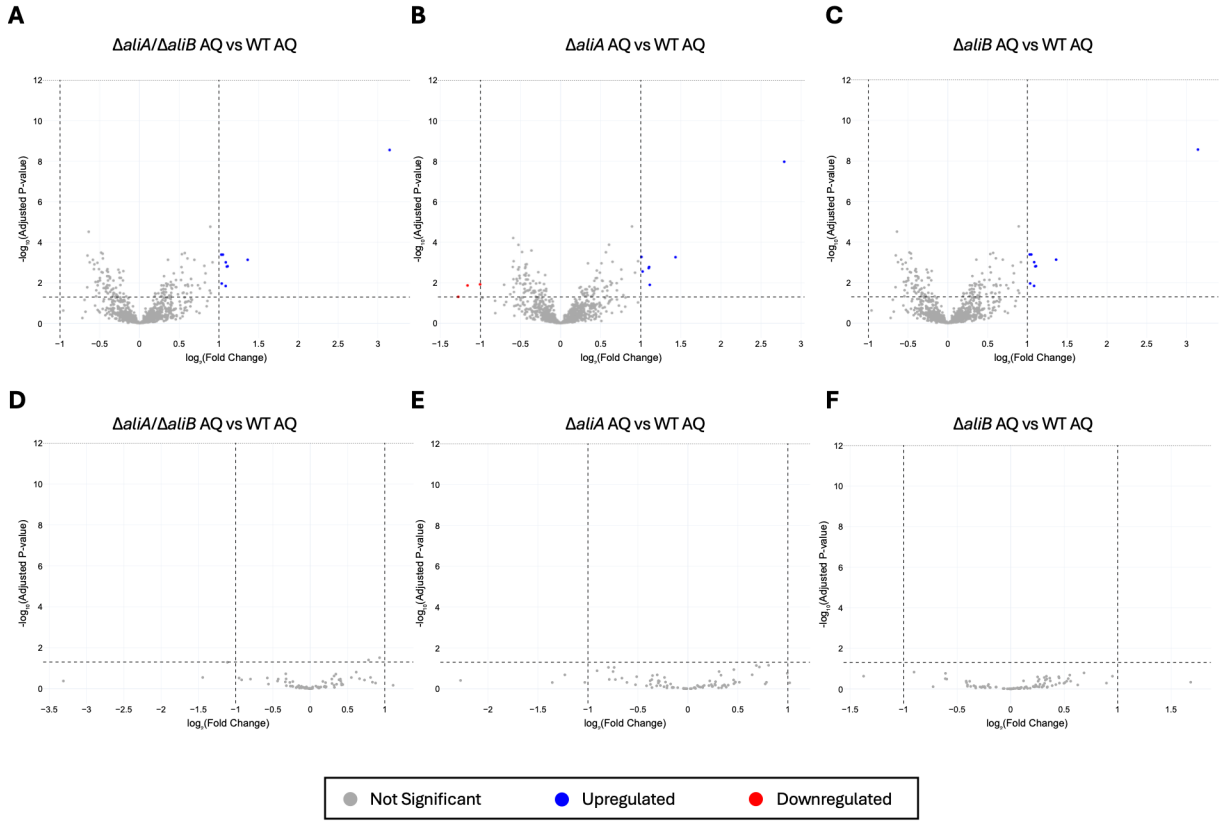

375

376 **Supplementary Fig. 3. Deletion of *aliA* and *aliB* induces comparatively modest changes in AQ-**
377 **associated non-lipoproteins.** Volcano plots show proteins in the AQ phase of (a,d) Δ*aliA*/Δ*aliB*, (b,e) Δ*aliA*,
378 and (c,f) Δ*aliB* compared to wild-type *Hfx. volcanii*. Panels a–c display AQ-associated proteins exhibiting
379 significant finite $\log_2$ fold enrichment in AQ relative to TX within each strain (i.e., detected in both phases).
380 Panels d–f display proteins detected exclusively in the AQ phase of at least one strain, resulting in negative

381 infinite $\log_2$ fold changes due to absence from the TX phase. Proteins with $|\log_2 FC| > 1$ and adjusted p-
382 value < 0.05 are considered significantly differentially abundant. No significantly differentially abundant
383 proteins were detected in panels d-f. Selected functional groups of differentially abundant proteins are
384 highlighted in distinct colors as indicated.

385 **DISCUSSION**

386 Protein lipidation occurs across all domains of life, yet the underlying mechanisms in archaea remain poorly
387 understood. Recently, we identified AliA and AliB as the first archaeal enzymes involved in lipoprotein
388 biogenesis, and showed their involvement in archaeal lipoprotein lipidation[43]. Although the two proteins are
389 paralogs, their functions are not redundant. Deletion of *aliA* or *aliB* in *Hfx. volcanii* led to distinct phenotypes
390 in both lipoprotein biogenesis and cell physiology, and cross-complementation did not restore the defects,
391 indicating that the two enzymes possess different enzymatic activities.

392 In this study, we further explored the functional differences between AliA and AliB by analyzing the lipidation
393 status of predicted lipoproteins in Δ*aliA*, Δ*aliB*, and Δ*aliA*/Δ*aliB*. We employed a large-scale Triton X-114
394 extraction, which enabled efficient separation of hydrophobic (TX phase, detergent phase) and hydrophilic
395 (AQ phase, aqueous phase) proteins from large culture samples. Subsequent MS of both fractions yielded
396 high proteome coverage, comparable to the most comprehensive single dataset in the Archaeal Proteome
397 Project (Supplementary Fig. 1a,b), underscoring TX-114 extraction as a powerful method for archaeal
398 proteomic analysis, particularly for enhancing the identification of membrane proteins. Overall, TX-114
399 extraction resulted in the expected separation of hydrophobic and hydrophilic proteins (Fig. 1a,b),
400 supporting its suitability for large-scale archaeal proteomic analysis. At the same time, a subset of predicted
401 lipoproteins and transmembrane proteins showed enrichment in the AQ phase, while some predicted
402 cytoplasmic proteins were detected in the TX phase. Such fractionation patterns likely reflect a combination
403 of imperfect predictions, minor cross-contamination, protein–protein interactions influencing phase
404 partitioning, or lower-than-expected hydrophobicity of specific lipid modifications or signal peptide H-
405 domains.

406 This approach also enabled the large-scale validation of archaeal lipoprotein predictions for the first time.
407 In total, 51 of 88 predicted lipoproteins quantified across all strains showed reduced abundance in the TX
408 phase - but not in the AQ phase – in at least one mutant (Fig. 3a), verifying their identity as lipoproteins.
409 Three previously experimentally confirmed lipoproteins were included in this group (Supplementary Data
410 2). In addition, the MS data corroborated earlier experimental findings for the predicted lipoprotein
411 HVO_1808 (Supplementary Data 2), indicating that the lipobox prediction might be false positive and that
412 the protein likely is not a true lipoprotein, further demonstrating the robustness of this validation strategy.
413 Considering that current archaeal lipoprotein prediction program is trained on a very limited number of
414 experimentally verified lipoproteins[62], the large-scale lipoprotein validation presented here provides a
415 critical dataset for refining and expanding these predictive models. It should be noted, however, that
416 lipoproteins for which failed lipid attachment leads to protein instability are not captured by our analysis, as
417 the applied filtering criteria exclude proteins with strongly reduced overall abundance. Future studies that
418 directly identify lipid-modified peptides by mass spectrometry will further strengthen lipoprotein validation.
419 Consistent with our previous findings that Δ*aliA* exhibited more severe phenotypes in growth, morphology,
420 and motility than Δ*aliB*[43], deletion of *aliA* affected substantially more lipoproteins than deletion of *aliB* (Fig.
421 3). Specifically, 47 of 51 validated lipoproteins showed reduced TX phase abundance in Δ*aliA*, whereas
422 only three lipoproteins were affected in Δ*aliB*, confirming the dominant role of AliA in *Hfx. volcanii* lipoprotein
423 lipidation (Fig. 3a, Supplementary Table 3).

424 Complementing the whole-proteome analysis, we examined a Tat-transported lipoprotein HVO_1705 both
425 as proof of concept and as a model substrate to further dissect the roles of AliA and AliB. In Δ*aliA* and
426 Δ*aliA*/Δ*aliB* strains HVO_1705 abundance was significantly reduced and the protein localized
427 predominantly to the cytoplasmic fraction (Fig. 4a,b), suggesting impaired translocation or clearance of the
428 non-lipidated form from the membrane by an unidentified quality-control system. In contrast, HVO_1705
429 expressed in Δ*aliB* remained largely membrane-associated, including both the mature form and a presumed
430 lipidated but non-cleaved intermediate (Fig. 4b). These observations indicate that AliB is not essential for
431 membrane localization and lipidation of HVO_1705 and may instead be involved in signal peptide cleavage
432 of lipoproteins. Analysis showed that a Tat-transported transmembrane protein, HVO_0844, was unaffected
433 by the deletion of either *ali* gene (Fig. 4c,d), confirming that these effects are specific to lipoproteins.

434 Consistent with the functional distinction between AliA and AliB, LC-MS analysis of lipids isolated from TX-
435 114 extracts further confirmed the dominant role of AliA in mediating thioether-linked archaeol modification
436 in *Hfx. volcanii*. The cleavage product of this modification (methylthio-archaeol) was absent in both Δ*aliA*
437 and Δ*aliA*/Δ*aliB* (Fig. 5). In contrast, deletion of *aliB* did not abolish the modification and instead resulted in
438 a slight, though not statistically significant, increase in the levels of thioether-linked archaeol (Fig. 5). This
439 trend is consistent with the modest upregulation of *aliA* expression observed in Δ*aliB* by both qPCR and
440 MS, suggesting potential regulatory crosstalk between AliA and AliB.

441 Beyond the altered abundance of *aliA* in the Δ*aliB* mutant, we observed differential abundance of multiple
442 non-lipoproteins in *ali* deletion strains (Fig. 6a-c). A considerable number of non-lipoproteins exemplifies
443 differential abundance in *ali* deletion strains, especially in the TX phase (Fig. 6a-c). Among these were
444 HVO_A0045 and HVO_2870, which were previously identified as proteins that most frequently co-occur
445 with archaeal lipoproteins[43], although how their respective functions relate to the lipoprotein biogenesis
446 pathway remains unclear. For HVO_A0045, an HtpX-like protease, reduced abundance in the mutants may
447 reflect its involvement in downstream processes of the Ali pathway, such as releasing membrane-
448 associated lipoproteins to the extracellular environment or activation of its self-cleavage activity in response
449 to membrane stress. Although membrane instability has not been reported for *ali* deletion strains, increased
450 outer membrane permeability has been observed in an *Escherichia coli* Δ*lgt* strain[63]. In contrast, HVO_2870,
451 a predicted AI-2E family transporter, showed increased abundance in the double knockout strain. Given
452 that AI-2E family proteins have been reported to function as Na^+ (Li^+)/H antiporters[61], this increase may
453 represent a compensatory response aimed at maintaining intracellular pH homeostasis in response to
454 membrane perturbations associated with *ali* deletion. Additional proteins showing differential abundance in
455 the mutants likely reflect broader consequences of Ali pathway disruption beyond lipoproteins themselves,
456 including downstream effects of impaired lipoprotein lipidation. Among these, a large number of transport
457 proteins were affected (Fig. 6a-f). In addition, the archaellin subunit proteins HVO_1210 exhibited reduced
458 abundance in all mutants (Fig. 6a-c), providing a molecular explanation for the motility defects observed in
459 these strains[43].

460 In summary, by combining large-scale quantitative proteomics with LC-MS analysis of thioether-linked
461 archaeol modifications in wild-type and *ali* mutant strains, we demonstrate that the vast majority of archaeal
462 lipoprotein lipidation in *Hfx. volcanii* is mediated by AliA, with AliB acting in a partially distinct role, likely
463 downstream of lipidation and potentially linked to signal peptide cleavage. Beyond defining the dominant
464 contribution of AliA, our quantitative proteomic analysis revealed changes in the abundance of multiple non-
465 lipoproteins in *ali* mutants, which may point to candidate components or regulators of the archaeal
466 lipoprotein biogenesis pathway. Importantly, this work substantially expands the number of experimentally
467 validated archaeal lipoproteins from fewer than ten to over fifty, providing a robust experimental framework
468 for refining lipoprotein prediction algorithms. Together, these data offer a valuable community resource for
469 studying protein lipidation across archaea, where the underlying mechanisms have remained largely
470 elusive.

471 **Supplementary Table 4. Plasmids, strains, and primers used in this study.**

	Name	Relevant characteristic(s)	Source of reference
Plasmids	pYH7	pTA963 carrying C-terminally myc-tagged *hvo_1705*	[43]
	pYH9	pTA963 carrying C-terminally myc-tagged *hvo_0844*	[43]
Strains	H53	Δ*pyrE2*/Δ*trpA*	[64]
	YH_113	H53 Δ*aliA*	[43]
	YH_57	H53 Δ*aliB*	[43]
	YH_93	H53 Δ*aliA*/Δ*aliB*	[43]
	YH_75	H53 containing pYH7	[43]
	YH_162	Δ*aliA* containing pYH7	[43]
	YH_83	Δ*aliB* containing pYH7	[43]
	YH_176	Δ*aliA*/Δ*aliB* containing pYH7	[43]
	YH_74	H53 containing pYH9	[43]
	YH_159	Δ*aliA* containing pYH9	[43]

	YH_82	Δ*aliB* containing pYH9	[43]
	YH_173	Δ*aliA*/Δ*aliB* containing pYH9	[43]
Primers	qPCR_*aliA*_F	CAACGGTAGCAGAGCGAATG	This study
	qPCR_*aliA*_R	TCCCCAGAAGTAGTGCAAGA	This study

472 **METHODS**

473 **Growth conditions.** Plasmids and strains used in this study are listed in Supplementary Table 4. *Hfx.*
474 *volcanii* strains were grown at 45 °C in liquid (orbital shaker at 250 rpm with an orbital diameter of 2.54 cm)
475 or on solid agar (containing 1.5% [w/v] agar) semi-defined Hv-Cab medium[65], supplemented with tryptophan
476 (Fisher Scientific) and uracil (Sigma) at a final concentration of 50 µg ml^{-1} unless otherwise noted. Uracil
477 was left out for strains carrying pTA963-based plasmids.

478 **Triton X-114 extraction.** A single colony of *Hfx. volcanii* was inoculated into 10 ml of liquid medium
479 supplemented with 200 µg ml^{-1} tryptophan. When the culture reached an OD_{600} of 0.3-0.8, it was used to
480 inoculate 1 l of secondary culture (starting OD_{600} = 0.004) in the same medium. Cells were harvested at
481 OD_{600} = 0.75-0.85 by centrifugation at 7,000 × g for 20 min at 4 °C. The cell pellets were resuspended in
482 7 ml PBS (pH 7.4) supplemented with 150 µl RQ1 RNase-Free DNase and protease inhibitor, resulting in
483 a final volume of approximately 10 ml. The cell suspensions were transferred to 15 ml Falcon tubes,
484 vortexed thoroughly, and lysed by five freeze-thaw cycles, alternating between freezing in liquid nitrogen
485 for 2 min and thawing at 37 °C for 20 min. Unlysed cells were removed by centrifugation at 9,000 × g for
486 20 min at 4 °C. Protein concentrations of the clarified lysates were determined using the Pierce™ BCA
487 Protein Assay Kit (Thermo Scientific). Triton X-114 extraction was performed as previously described with
488 slight modifications[43]. Briefly, 1 ml ice-cold 20% Triton X-114 was added to 9 ml of clarified lysate containing
489 the desired amount of protein in a 15 ml Falcon tube. The mixture was gently mixed on a rotator at 4˚C for
490 3 h and then centrifuged at 9,000 × g for 10 min at 4 °C to remove precipitates. The supernatant was
491 transferred to a fresh tube and incubated at 37 °C for 20 min to induce detergent phase separation, followed
492 by centrifugation at 9,000 × g for 10 min at room temperature. The resulting phase separation yielded
493 approximately 9 ml of aqueous (AQ) phase and ~1 ml of detergent (TX) phase. The AQ phase was

494 transferred to a new 15 ml Falcon tube, and 889 ul of ice-cold 20% TX-114 was added for washing. The TX
495 phase was adjusted to a final volume of 10 ml with PBS for washing. Both samples were incubated on ice
496 for 10 min until clear and then at 37 °C for 20 min until the solution became turbid. Phase-separated
497 samples were centrifuged again at 9,000 × g for 10 min at room temperature. The washed AQ phase was
498 transferred to a new tube and stored at −80 °C for further use. For the washed TX phase, the supernatant
499 was removed, 10 ml methanol was added, and samples were stored at −80 °C overnight to precipitate
500 proteins. Protein precipitates were collected the following day by centrifugation at 10,000 × g for 10 min
501 and the pellet was stored at −80 °C for downstream analysis.

502 **Mass spectrometry of proteins in TX and AQ phases.** Triton X-114 extraction was performed as
503 described above, starting with cell lysates containing 60 mg of total proteins. Protein precipitates from the
504 TX phase were resuspended with 200 µl or 300 µl PBS buffer with protease inhibitor. The protein
505 concentration was measured using the BCA Protein Assay Kit. Mass spectrometry sample preparation was
506 performed as previously described[66]. Briefly, 50 µg of protein from each sample was reduced with DTT,
507 alkylated with iodoacetamide, and digested with trypsin overnight at 37 °C using S-trap mini spin columns
508 (ProtiFi) following manufacturer's instructions. Resulting peptides were eluted, dried in a vacuum centrifuge,
509 and desalted using C18 stage-tips as described previously[67]. Mass spectrometric analysis was performed,
510 as described in Schiller et al. (2024)[66], on an Orbitrap Eclipse™ after separation on a nanoEase M/Z Peptide
511 BEH C18 column.

512 **Proteomics data processing and statistical analysis.** Peptide identification and quantification with
513 statistical post-processing followed the same procedures as in Chatterjee et al. (2025)[68], except that a
514 newer version of the theoretical proteome was used, from March 28th, 2023
515 (https://doi.org/10.5281/zenodo.7794769), containing 4222 proteins. Briefly, peptides were identified using
516 MSFragger, X!Tandem, and MS-GF+ via Ursgal[69] and quantified through FlashLFQ[70]. Peptide abundances
517 were further processed through MSstats[71], including log transformation, median normalization, integration
518 on protein level, and calculation of fold-changes (FCs) with corresponding p-values that were adjusted for
519 multiple testing. Log_2FCs were considered statistically significant if their associated adjusted p-value was
520 ≤0.05.

521 To compare the distribution of different protein groups in the TX and AQ phases, the whole theoretical
522 proteome was used as an input for the prediction of lipoproteins (comprising lipoproteins processed through
523 the Sec as well as the Tat pathway) through SignalP (v. 6.0)[62], transmembrane domains through
524 DeepTMHMM (v. 1.0.44)[72], and type III signal peptides through FlaFind (v. 1.2)[73]. Proteins were assigned
525 to the predicted lipoprotein group, if SignalP results for LIPO(Sec/SPII) or TATLIPO(Tat/SPII) had a
526 confidence of ≥0.9, and if they were not FlaFind positive. The ≥2 TM protein group was defined by
527 DeepTMHMM results that predicted at least two TM regions, as long as these proteins were not FlaFind
528 positive or exhibited SignalP predictions different from "Other". All proteins that were FlaFind negative and
529 had "Other" as a SignalP prediction, which in combination means that they do not contain any of the
530 secretion signals and had no predicted TM regions, were designated as predicted cytoplasmic proteins.

531 MSstats results were grouped based on these predicted protein groups, and figures were generated using
532 custom Python scripts (https://doi.org/10.5281/zenodo.18783633), employing the following packages:
533 Pandas[74], SciPy[75], Plotly[76], and Matplotlib[77]. Comparisons between the groups were assessed for statistical
534 significance employing a one-way ANOVA test with Tukey's post-hoc test, using the SciPy stats package.
535 Protein groups were excluded from analyses downstream of MSstats if all constituent proteins were
536 quantified through proteotypic peptides.

537 **Lipid processing and analysis.** A single colony of *Hfx. volcanii* was inoculated into 5 ml of liquid medium
538 and grown to an OD_{600} of 0.3-0.8. This culture was then used to inoculate 25 ml of fresh medium at a
539 starting OD_{600} = 0.01. Cells were harvested at an OD_{600} = 0.65-0.75 by centrifugation at 7,000 × g for 20 min
540 at 4 °C. Core lipids were obtained from the harvested biomass by base hydrolysis as previously described[43].
541 For the methyl iodide treatment, lipoproteins were extracted from 80 mg total proteins using Triton X-114.
542 Following extraction, lipoprotein samples were treated with methyl iodide to release thioether bound lipids
543 as previously described[43].

544 Core lipids and compounds released from methyl-iodide treatment were analyzed on an Agilent 1260 Infinity
545 II series high-performance liquid chromatography instrument coupled to an Agilent G6125B single
546 quadrupole mass spectrometer. Samples were ionized with electrospray ionization and detected in positive
547 mode with the following parameters: 8.0 l/min drying gas flow rate, 35 psi nebulizer pressure,

548 3,000 V capillary voltage, and either a 300 °C drying gas temperature (for core lipids) or 250 °C drying gas
549 temperature (for methylthio-archaeol analysis). Core lipids were separated on a Kinetex 1.7 µm XB-C18
550 100 Å LC column (150 × 2.1 mm), and lipids released from methyl iodide treated lipoproteins were
551 separated on an Agilent Poroshell 120 EC-C18 column (1.9 µm, 2.1 × 150 mm) as described in our previous
552 work[43]. For quantification of the mass of methylthio-archaeol released from each sample, the peak areas
553 of m/z = 683.7, 700.8, and 705.7, (corresponding to the [M+H]+, [M+NH4]+, [M+Na]+ adducts of methylthio-
554 archaeol) were calculated and summed using Agilent MassHunter B.08.00 and inspected manually to
555 confirm the proper integration of extracted ion peaks. The peak area was converted to the mass of
556 methylthio-archaeol injected by the use of a 10-point standard curve as described in our previous work.
557 The methylthio-archaeol (diphytanylglyceryl methyl thioether) standard was synthesized by Pharmaron, Inc.
558 via a synthesis scheme previously described in Hong et al. (2025)[43].

559 **Quantitative PCR analysis of *aliA* expression.** Three biological replicates of Δ*aliB* and wild type were
560 collected at OD_{600} = 0.8 for each comparison, with 0.5 ml liquid cultures of each strain harvested and
561 pelleted at 4,900 × g for 6 min. RNA was extracted using the Qiagen RNeasy Plus Micro Kit (Qiagen) on
562 the QIAcube Connect automated platform (Qiagen), with lysates homogenized via QIAshredder Columns
563 (Qiagen). RNA extracts were subjected to DNase digestion using the RNase-Free DNase kit (Qiagen) and
564 further purified by RNeasy MinElute Cleanup Kit (Qiagen). RNA concentrations were measured with Qubit
565 RNA Broad Range Assay Kits (Invitrogen), and integrity assessed using RNA ScreenTape on a 4200
566 Tapestation (Agilent). All samples had RINe values between 8.4-8.8. cDNA was synthesized from 1 µg RNA
567 using the ProtoScript II First Strand cDNA Synthesis Kit (New England BioLabs) with random primers;
568 parallel negative controls without reverse transcriptase (-RT) were prepared. Primers for *Hfx. volcanii* gene
569 *aliA* (Supplementary Table 4) were designed using Primer3[78] and synthesized as RxnReady™ primers (IDT).
570 Primers for the internal reference gene *eif1a* from prior studies were used[79]. qRT PCR reactions (20 µl)
571 contained 2× iTaq Universal SYBR Green Supermix (Bio-Rad), 5% DMSO, 300 nM primers, and 8 µl of
572 1:25 diluted cDNA. No-template (NTC) and -RT controls were included; reactions were considered
573 acceptable if ΔCt ≤10 between sample and both controls. Efficiencies for *aliA* and *eif1a* primer sets were
574 determined via standard curves and were 93.0% and 88.7% respectively. Each reaction included three
575 biological replicates, each with three technical replicates, run on a QuantStudio 3 Real-Time PCR System

576 (Applied Biosystems). Thermal cycling conditions were: 95 °C for 2 min, then 40 cycles of 95 °C for 15 s
577 and 60 °C for 30 s. SYBR Green fluorescence (Rox normalized) was recorded at each cycle's end, and the
578 default melt curve program following the qPCR run verified primer specificity. Relative expression was
579 calculated in Excel using the Pfaffl method[80], normalizing to *eif1a*, and compared to wild-type controls to
580 determine differential expression.

581 **Immunoblotting.** A single colony was used to inoculate a 5 ml liquid culture. At an OD_{600} of 0.75-0.80, cells
582 from 4 ml liquid culture were harvested by centrifugation at 4,300 x g for 10 min at 4 °C. Cell pellets were
583 then resuspended in 200 µl PBS buffer with 1 mM AEBSF and lysed by freezing (with liquid nitrogen or
584 ethanol with dry ice) and thawing (at 37 °C) four times. 20 µl RQ1 RNase-Free DNase (Promega) was
585 added to cell lysates, and the mixture was incubated at 37 °C for 30 min to degrade DNA. Unlysed cells
586 were removed by centrifugation at 4,300 x g for 10 min at 4 °C, and the supernatant was transferred to a
587 new tube for subsequent fractionation. To fractionate the lysates, 200 µl of cleared supernatant was
588 subjected to ultracentrifugation at 81,000 rpm (231,472 × g) for 30 min at 4 °C using a TLA-100.2 fixed-
589 angle rotor in a Beckman Coulter Optima MAX-TL ultracentrifuge. The resulting supernatant (cytoplasmic
590 fraction) was transferred to a new ultracentrifuge tube, and the pellet (membrane fraction) was resuspended
591 in 200 µl ice-cold PBS with 1mM AEBSF. Both fractions were centrifuged again at 81,000 rpm for 30 min at
592 4 °C. Pellets were then resuspended in 200 µl PBS with 1mM AEBSF, while the cytoplasmic fraction was
593 transferred to a new tube.

594 10 µl of HVO_1705 samples and 21 µl of HVO_0844 samples were supplemented with 50 mM dithiothreitol
595 and 1x NuPAGE LDS Sample Buffer. PBS was added to adjust each sample to a final volume of 30 µl.
596 Samples were incubated at 70 °C for 10 min, after which 27 µl of each sample was loaded onto NuPAGE
597 10%, Bis-Tris mini gels (8 cm x 8 cm, 1.0 mm x 10 wells) with NuPAGE MOPS SDS Running Buffer. After
598 electrophoresis, proteins were transferred to a polyvinylidene difluoride (PVDF) membrane (Millipore) using
599 a semi-dry transfer apparatus (BioRad) at 15 V for 30 min. Subsequently, the membrane was stained with
600 Ponceau S Staining Solution (Cell Signaling Technology) to verify the successful protein transfer. The
601 membrane was then washed for 10 min twice in PBS buffer and blocked for 1 h in 5% non-fat milk
602 (LabScientific) in PBST buffer (PBS with 1% Tween-20). After blocking, the membrane was washed twice

603 in PBST and once in PBS. For detection of the myc tag, anti-Myc antibody (9E10, UPenn Cell Center
604 Service) was diluted 1,000 times with PBS buffer containing 3% bovine serum albumin, which was then
605 used to incubate the membrane overnight at 4 °C. Subsequently, the membrane was washed twice in PBST
606 and once in PBS, followed by a 45-min incubation at room temperature with the secondary antibody solution
607 (Amersham ECL anti-mouse IgG, horseradish peroxidase-linked whole antibody, from sheep (Cytiva)
608 diluted 10,000 times in PBS containing 10% non-fat milk). After incubation, the membrane was washed
609 three times in PBST and once in PBS. HRP activity was assessed using the Amersham ECL Prime Western
610 Blotting Detection Reagent (GE). Membranes were imaged using an Amersham Imager 600, with image
611 analysis conducted using the Amersham Imager 600 Analysis software.

612 **DATA AVAILABILITY**

613 The LC-MS raw data and quantification for lipid analysis can be accessed through the Stanford Digital
614 Repository [https://purl.stanford.edu/nk164tn8116]. The MS raw files generated for the proteomic analysis
615 in this study have been deposited to the ProteomeXchange Consortium via the PRIDE partner
616 repository with the dataset identifier PXD074718, and all identification and quantification results have been
617 included in the deposited dataset. Raw and processed qPCR data are available at
618 [https://doi.org/10.5281/zenodo.18783633].

619 All other data supporting the findings of this study are provided within the paper and its supplementary
620 information files. Source data are provided with this paper.

621 **CODE AVAILABILITY**

622 All scripts for the identification and quantification of peptides and proteins from MS datasets are made
623 available through the Archaeal Proteome Project (http://archaealproteomeproject.org) and its associated
624 GitHub repository (https://github.com/arcpp/ArcPP v1.4.0). Custom Python pipelines used for data filtering
625 and figure generation is available at Zenodo under the identifier DOI: 10.5281/zenodo.18783632
626 [https://doi.org/10.5281/zenodo.18783633].

627 **REFERENCES**

628 1. Jiang, H. *et al.* Protein Lipidation: Occurrence, Mechanisms, Biological Functions, and Enabling
629 Technologies. *Chem. Rev.* **118**, 919–988 (2018).
630 2. Banahene, N. *et al.* Chemical Proteomics Strategies for Analyzing Protein Lipidation Reveal the
631 Bacterial O-Mycoloylome. *J. Am. Chem. Soc.* **146**, 12138–12154 (2024).
632 3. Braun, V. & Hantke, K. Lipoproteins: structure, function, biosynthesis. in *Bacterial Cell Walls and*
633 *Membranes* 39–77 (Springer, 2019).
634 4. Storf, S. *et al.* Mutational and bioinformatic analysis of haloarchaeal lipobox-containing proteins.
635 *Archaea* **2010**, 410975 (2010).
636 5. Ding, W. *et al.* The Biosynthesis and Applications of Protein Lipidation. *Chem. Rev.* **124**, 12176–12212
637 (2024).
638 6. Spang, A. *et al.* Complex archaea that bridge the gap between prokaryotes and eukaryotes. *Nature*
639 **521**, 173–179 (2015).
640 7. Zaremba-Niedzwiedzka, K. *et al.* Asgard archaea illuminate the origin of eukaryotic cellular complexity.
641 *Nature* **541**, 353–358 (2017).
642 8. Da Cunha, V., Gaïa, M. & Forterre, P. The expanding Asgard archaea and their elusive relationships
643 with Eukarya. *mLife* **1**, 3–12 (2022).
644 9. Baker, B. J. *et al.* Diversity, ecology and evolution of Archaea. *Nat. Microbiol.* **5**, 887–900 (2020).
645 10. Jung, J., Kim, J.-S., Taffner, J., Berg, G. & Ryu, C.-M. Archaea, tiny helpers of land plants. *Comput.*
646 *Struct. Biotechnol. J.* **18**, 2494–2500 (2020).
647 11. Pfeifer, K. *et al.* Archaea biotechnology. *Biotechnol. Adv.* **47**, 107668 (2021).
648 12. Haque, R. U., Paradisi, F. & Allers, T. *Haloferax volcanii* for biotechnology applications: challenges,
649 current state and perspectives. *Appl. Microbiol. Biotechnol.* **104**, 1371–1382 (2020).
650 13. Kobayashi, T., Nishizaki, R. & Ikezawa, H. The presence of GPI-linked protein(s) in an
651 archaeobacterium, *Sulfolobus acidocaldarius*, closely related to eukaryotes. *Biochim. Biophys. Acta*
652 *BBA - Gen. Subj.* **1334**, 1–4 (1997).
653 14. Kates, M., Palameta, B., Joo, C. N., Kushner, D. J. & Gibbons, N. E. Aliphatic Diether Analogs of
654 Glyceride-Derived Lipids. IV. The Occurrence of Di-O-dihydrophytylglycerol Ether Containing Lipids in
655 Extremely Halophilic Bacteria*. *Biochemistry* **5**, 4092–4099 (1966).

656 15. Kates, M., Wassef, M. K. & Kushner, D. J. Radioisotopic studies on the biosynthesis of the glyceryl
657 diether lipids of Halobacterium cutirubrum. *Can. J. Biochem.* **46**, 971–977 (1968).
658 16. Pugh, E. L. & Kates, M. Acylation of proteins of the archaebacteria *Halobacterium cutirubrum* and
659 *Methanobacterium thermoautotrophicum*. *Biochim. Biophys. Acta BBA - Biomembr.* **1196**, 38–44
660 (1994).
661 17. Kikuchi, A., Sagami, H. & Ogura, K. Evidence for Covalent Attachment of Diphytanylglyceryl Phosphate
662 to the Cell-surface Glycoprotein of Halobacterium halobium *. *J. Biol. Chem.* **274**, 18011–18016 (1999).
663 18. Sagami, H., Kikuchi, A., Ogura, K., Fushihara, K. & Nishino, T. Novel Isoprenoid Modified Proteins in
664 Halobacteria. *Biochem. Biophys. Res. Commun.* **203**, 972–978 (1994).
665 19. Sagami, H., Kikuchi, A. & Ogura, K. A novel type of protein modification by isoprenoid-derived materials.
666 Diphytanylglycerylated proteins in Halobacteria. *J. Biol. Chem.* **270**, 14851–14854 (1995).
667 20. Abdul Halim, M. F. *et al. Haloferax volcanii* archaeosortase is required for motility, mating, and C-
668 terminal processing of the S-layer glycoprotein. *Mol. Microbiol.* **88**, 1164–1175 (2013).
669 21. Abdul Halim, M. F. *et al.* Permuting the PGF Signature Motif Blocks both Archaeosortase-Dependent
670 C-Terminal Cleavage and Prenyl Lipid Attachment for the Haloferax volcanii S-Layer Glycoprotein. *J.*
671 *Bacteriol.* **198**, 808–815 (2016).
672 22. Abdul Halim, M. F. *et al.* Lipid anchoring of archaeosortase substrates and midcell growth in
673 haloarchaea. *mBio* **11**, 10.1128/mbio.00349-20 (2020).
674 23. Konrad, Z. & Eichler, J. Lipid modification of proteins in Archaea: attachment of a mevalonic acid-based
675 lipid moiety to the surface-layer glycoprotein of Haloferax volcanii follows protein translocation.
676 *Biochem. J.* **366**, 959–964 (2002).
677 24. Kandiba, L., Guan, Z. & Eichler, J. Lipid modification gives rise to two distinct *Haloferax volcanii* S-layer
678 glycoprotein populations. *Biochim. Biophys. Acta BBA - Biomembr.* **1828**, 938–943 (2013).
679 25. Siliakus, M. F., van der Oost, J. & Kengen, S. W. M. Adaptations of archaeal and bacterial membranes
680 to variations in temperature, pH and pressure. *Extremophiles* **21**, 651–670 (2017).
681 26. Gattinger, A., Schloter, M. & Munch, J. C. Phospholipid etherlipid and phospholipid fatty acid
682 fingerprints in selected euryarchaeotal monocultures for taxonomic profiling. *FEMS Microbiol. Lett.* **213**,
683 133–139 (2002).

684 27. Lombard, J., López-García, P. & Moreira, D. Phylogenomic investigation of phospholipid synthesis in
685 archaea. *Archaea* **2012**, 630910 (2012).
686 28. Villanueva, L. *et al.* Bridging the membrane lipid divide: bacteria of the FCB group superphylum have
687 the potential to synthesize archaeal ether lipids. *ISME J.* **15**, 168–182 (2021).
688 29. Sinninghe Damsté, J. S. *et al.* Dominance of mixed ether/ester, intact polar membrane lipids in five
689 species of the order *Rubrobacterales*: Another group of bacteria not obeying the “lipid divide”. *Syst.*
690 *Appl. Microbiol.* **46**, 126404 (2023).
691 30. Sahonero-Canavesi, D. X. *et al.* Disentangling the lipid divide: Identification of key enzymes for the
692 biosynthesis of membrane-spanning and ether lipids in Bacteria. *Sci. Adv.* **8**, eabq8652 (2022).
693 31. Abdul Halim, M. F., Stoltzfus, J. D., Schulze, S., Hippler, M. & Pohlschroder, M. ArtA-dependent
694 processing of a Tat substrate containing a conserved tripartite structure that is not localized at the C
695 terminus. *J. Bacteriol.* **199**, (2017).
696 32. Babu, M. M. *et al.* A database of bacterial lipoproteins (DOLOP) with functional assignments to
697 predicted lipoproteins. *J. Bacteriol.* **188**, 2761–2773 (2006).
698 33. El Rayes, J., Rodríguez-Alonso, R. & Collet, J.-F. Lipoproteins in Gram-negative bacteria: new insights
699 into their biogenesis, subcellular targeting and functional roles. *Curr. Opin. Microbiol.* **61**, 25–34 (2021).
700 34. Nguyen, M.-T., Matsuo, M., Niemann, S., Herrmann, M. & Götz, F. Lipoproteins in Gram-positive
701 bacteria: abundance, function, fitness. *Front. Microbiol.* **11**, 582582 (2020).
702 35. Thompson, B. J. *et al.* Investigating lipoprotein biogenesis and function in the model Gram-positive
703 bacterium Streptomyces coelicolor. *Mol. Microbiol.* **77**, 943–957 (2010).
704 36. Gan, K., Gupta, S. D., Sankaran, K., Schmid, M. B. & Wu, H. C. Isolation and characterization of a
705 temperature-sensitive mutant of Salmonella typhimurium defective in prolipoprotein modification. *J.*
706 *Biol. Chem.* **268**, 16544–16550 (1993).
707 37. Tokunaga, M., Loranger, J. M. & Wu, H. C. Prolipoprotein modification and processing enzymes in
708 Escherichia coli. *J. Biol. Chem.* **259**, 3825–3830 (1984).
709 38. Gupta, S. D. & Wu, H. C. Identification and subcellular localization of apolipoprotein *N*-acyltransferase
710 in *Escherichia coli*. *FEMS Microbiol. Lett.* **78**, 37–42 (1991).

711 39. John H Gardiner, I. V. *et al.* Lipoprotein *N*-acylation in *Staphylococcus aureus* is catalyzed by a two-
712 component acyl transferase system. *mBio* **11**, e01619 (2020).
713 40. Armbruster, K. M. & Meredith, T. C. Identification of the lyso-form *N*-acyl intramolecular transferase in
714 low-GC firmicutes. *J. Bacteriol.* **199**, 10.1128/jb.00099-17 (2017).
715 41. Pohlschroder, M., Pfeiffer, F., Schulze, S. & Halim, M. F. A. Archaeal cell surface biogenesis. *FEMS*
716 *Microbiol. Rev.* **42**, 694–717 (2018).
717 42. Giménez, M. I., Dilks, K. & Pohlschröder, M. *Haloferax volcanii* twin-arginine translocation substates
718 include secreted soluble, C-terminally anchored and lipoproteins. *Mol. Microbiol.* **66**, 1597–1606 (2007).
719 43. Hong, Y. *et al.* Uncovering the prevalence, key biogenesis enzymes, and biological significance of
720 archaeal lipoproteins. *Nat. Commun.* **16**, 8411 (2025).
721 44. Mattar, S. *et al.* The primary structure of halocyanin, an archaeal blue copper protein, predicts a lipid
722 anchor for membrane fixation. *J. Biol. Chem.* **269**, 14939–14945 (1994).
723 45. Tschumi, A. *et al.* Functional analyses of mycobacterial lipoprotein diacylglyceryl transferase and
724 comparative secretome analysis of a mycobacterial lgt mutant. *J. Bacteriol.* **194**, 3938–3949 (2012).
725 46. Dautin, N. *et al.* Role of the unique, non-essential phosphatidylglycerol::prolipoprotein diacylglyceryl
726 transferase (Lgt) in *Corynebacterium glutamicum*. *Microbiology* **166**, 759–776 (2020).
727 47. Mao, G. *et al.* Crystal structure of *E. coli* lipoprotein diacylglyceryl transferase. *Nat. Commun.* **7**, 10198
728 (2016).
729 48. Sankaran, K. *et al.* Roles of histidine-103 and tyrosine-235 in the function of the prolipoprotein
730 diacylglyceryl transferase of *Escherichia coli*. *J. Bacteriol.* **179**, 2944–2948 (1997).
731 49. González de la Vara, L. E. & Alfaro, B. L. Separation of membrane proteins according to their
732 hydropathy by serial phase partitioning with Triton X-114. *Anal. Biochem.* **387**, 280–286 (2009).
733 50. Hooper, N. M. & Bashir, A. Glycosyl-phosphatidylinositol-anchored membrane proteins can be
734 distinguished from transmembrane polypeptide-anchored proteins by differential solubilization and
735 temperature-induced phase separation in Triton X-114. *Biochem. J.* **280**, 745–751 (1991).
736 51. Mathias, R. A. *et al.* Triton X-114 phase separation in the isolation and purification of mouse liver
737 microsomal membrane proteins. *Methods* **54**, 396–406 (2011).

738 52. Kittelberger, R., Hansen, M. F., Hilbink, F., de Lisle, G. W. & Cloeckaert, A. Selective extraction of
739 bacterial macromolecules by temperature-induced phase separation in Triton X-114 solution. *J.*
740 *Microbiol. Methods* **24**, 81–92 (1995).
741 53. Métivier, A. *et al.* Triton X-114 phase partitioning for the isolation of a pediocin-like bacteriocin from
742 Carnobacterium divergens. *Lett. Appl. Microbiol.* **30**, 42–46 (2000).
743 54. Kwok, Y. *et al.* Rapid isolation and characterization of bacterial lipopeptides using liquid
744 chromatography and mass spectrometry analysis. *Proteomics* **11**, 2620–2627 (2011).
745 55. Schulze, S. *et al.* The Archaeal Proteome Project advances knowledge about archaeal cell biology
746 through comprehensive proteomics. *Nat. Commun.* **11**, 3145 (2020).
747 56. Schulze, S., Pfeiffer, F., Garcia, B. A. & Pohlschroder, M. Comprehensive glycoproteomics shines new
748 light on the complexity and extent of glycosylation in archaea. *PLoS Biol.* **19**, e3001277 (2021).
749 57. Franco, P. H. C. *et al.* Proteome characterization of single gene deletion mutants lacking zinc finger μ-
750 proteins in *Haloferax volcanii*. *microLife* uqag005 (2026) doi:10.1093/femsml/uqag005.
751 58. Makarova, K. S., Wolf, Y. I. & Koonin, E. V. Archaeal clusters of orthologous genes (arCOGs): an update
752 and application for analysis of shared features between Thermococcales, Methanococcales, and
753 Methanobacteriales. *Life* **5**, 818–840 (2015).
754 59. Makarova, K. S., Wolf, Y. I. & Koonin, E. V. Towards functional characterization of archaeal genomic
755 dark matter. *Biochem. Soc. Trans.* **47**, 389–398 (2019).
756 60. Rettner, R. E. & Saier Jr., M. H. The Autoinducer-2 Exporter Superfamily. *Microb. Physiol.* **18**, 195–205
757 (2010).
758 61. Dong, P. *et al.* A UPF0118 family protein with uncharacterized function from the moderate halophile
759 Halobacillus andaensis represents a novel class of Na+(Li+)/H+ antiporter. *Sci. Rep.* **7**, 45936 (2017).
760 62. Teufel, F. *et al.* SignalP 6.0 predicts all five types of signal peptides using protein language models. *Nat.*
761 *Biotechnol.* **40**, 1023–1025 (2022).
762 63. Diao, J. *et al.* Inhibition of Escherichia coli Lipoprotein Diacylglyceryl Transferase Is Insensitive to
763 Resistance Caused by Deletion of Braun's Lipoprotein. *J. Bacteriol.* https://doi.org/10.1128/JB.00149-
764 21 (2021) doi:10.1128/JB.00149-21.

765 64. Allers, T., Ngo, H.-P., Mevarech, M. & Lloyd, R. G. Development of additional selectable markers for
766 the halophilic archaeon *Haloferax volcanii* based on the *leuB* and *trpA* genes. *Appl. Environ. Microbiol.*
767 **70**, 943–953 (2004).
768 65. de Silva, R. T. *et al.* Improved growth and morphological plasticity of Haloferax volcanii. *Microbiology*
769 **162**, (2021).
770 66. Schiller, H. *et al.* Identification of structural and regulatory cell-shape determinants in *Haloferax volcanii*.
771 *Nat. Commun.* **15**, 1414 (2024).
772 67. Rappsilber, J., Mann, M. & Ishihama, Y. Protocol for micro-purification, enrichment, pre-fractionation
773 and storage of peptides for proteomics using StageTips. *Nat. Protoc.* **2**, 1896–1906 (2007).
774 68. Chatterjee, P. *et al.* Quorum sensing mediates morphology and motility transitions in the model
775 archaeon Haloferax volcanii. *mBio* **16**, e00906-25 (2025).
776 69. Kremer, L. P. M., Leufken, J., Oyunchimeg, P., Schulze, S. & Fufezan, C. Ursgal, Universal Python
777 Module Combining Common Bottom-Up Proteomics Tools for Large-Scale Analysis. *J. Proteome Res.*
778 **15**, 788–794 (2016).
779 70. Millikin, R. J., Shortreed, M. R., Scalf, M. & Smith, L. M. Fast, Free, and Flexible Peptide and Protein
780 Quantification with FlashLFQ. *Methods Mol. Biol. Clifton NJ* **2426**, 303–313 (2023).
781 71. Kohler, D. *et al.* MSstats Version 4.0: Statistical Analyses of Quantitative Mass Spectrometry-Based
782 Proteomic Experiments with Chromatography-Based Quantification at Scale. *J. Proteome Res.* **22**,
783 1466–1482 (2023).
784 72. Hallgren, J. *et al.* DeepTMHMM predicts alpha and beta transmembrane proteins using deep neural
785 networks. 2022.04.08.487609 Preprint at https://doi.org/10.1101/2022.04.08.487609 (2022).
786 73. Esquivel, R. N., Xu, R. & Pohlschroder, M. Novel Archaeal Adhesion Pilins with a Conserved N
787 Terminus. *J. Bacteriol.* **195**, 3808–3818 (2013).
788 74. McKinney, W. Data Structures for Statistical Computing in Python. *SciPy 2010*
789 https://doi.org/10.25080/Majora-92bf1922-00a (2010) doi:10.25080/Majora-92bf1922-00a.
790 75. Virtanen, P. *et al.* SciPy 1.0: fundamental algorithms for scientific computing in Python. *Nat. Methods*
791 **17**, 261–272 (2020).
792 76. Inc, P. T. Collaborative data science. https://plot.ly (2015).

77. Hunter, J. D. Matplotlib: A 2D Graphics Environment. *Comput. Sci. Eng.* **9**, 90–95 (2007).
78. Untergasser, A. *et al.* Primer3—new capabilities and interfaces. *Nucleic Acids Res.* **40**, e115 (2012).
79. Cote, J. A. *et al.* A Two-Component Regulatory System Mediates Quorum Sensing–Dependent Morphology and Motility Transitions in the Archaeon Haloferax volcanii. 2025.11.10.687552 Preprint at https://doi.org/10.1101/2025.11.10.687552 (2025).
80. Pfaffl, M. W. A new mathematical model for relative quantification in real-time RT–PCR. *Nucleic Acids Res.* **29**, e45 (2001).

ACKNOWLEDGEMENTS

We gratefully acknowledge the quantitative proteomics analysis conducted by Dr. Jeremy L. Balsbaugh and Dr. Jennifer C. Liddle of the UConn Proteomics & Metabolomics Facility, a component of the Center for Open Research Resources and Equipment at the University of Connecticut. The authors would like to acknowledge the NIH S10 High-End Instrumentation Award 1S10-OD028445-01A1, which supported this work by providing funds to acquire the Orbitrap Eclipse Tribrid mass spectrometer housed in the University of Connecticut Proteomics & Metabolomics Facility. We also gratefully acknowledge Research Computing at the Rochester Institute of Technology (RIT) for providing computational resources and support that have contributed to the research results reported in this publication. We thank the members of the Proteomics Core Facility of the Max-Planck-Institute of Biochemistry (RRID:SCR_025745) for their assistance with preliminary mass spectrometric analyses of samples containing myc-tagged HVO_1705. We are grateful to Dr. Kira S. Makarova for her insights and guidance on the annotation of specific arCOGs.

Y.H., J.C., and M.P. were supported by the National Science Foundation Grant MBC-2222076 and the University of Pennsylvania Research Fund grant. P.V.W. and A.A.G. were supported by the National Science Foundation Grant EAR-1752564. S.S. gratefully acknowledges support from the College of Science at RIT. S.K. was supported by the Emerson Summer Undergraduate Research Fellowship.